ÉCOLE POLYTECHNIQUE FÉDÉRALE DE LAUSANNE (EPFL)
UNISANTÉ - CENTRE UNIVERSITAIRE DE MÉDECINE GÉNÉRALE
ET DE SANTÉ PUBLIQUE - LAUSANNE
MASTER PROJECT SIE

EPFL

unisanté

Centre universitaire de médecine générale
et santé publique · Lausanne

Understanding the reactivity of the oxidative potential measured by the FOX assay towards ambient gases and particulate matter

Estelle Montet

Under the supervision of Dr. Guillaume Suarez, Dr. Jean-Jacques
Sauvain, Dr. Florian Breider, and Prof. David Vernez

Lausanne, 26th August 2022

Abstract

Air pollution has a significant impact on health and can is associated with increased mortality. Oxidative potential (OP) shows promising results as an air pollution metric because it better captures the toxicological effect of particulate matter (PM) than PM mass concentration. In this work, an on-line ambient air OP measuring device prototype based on the ferric-orange xylenol assay (FOX) (OP^{FOX}) is improved and used to assess the OP^{FOX} assay sensitivity to different gases and ambient air conditions. The FOX assay is based on the Fe^{2+} oxidation into Fe^{3+} and complexation with orange xylenol. The time evolution of the complex absorbance at 580 nm evolution is used to express the OP. The OP measuring device prototype operates sequentially: (i) FOX addition into the bubbling cell, (ii) air sample (possibly containing oxidants on the particles or in the gaseous phase) bubbling into the FOX solution (oxidation of Fe^{2+} starts during this step), (iii) FOX circulation to the optical detection cell, and (iv) measurement phase.

In a first stage, the OP^{FOX} measurement device prototype was characterized towards H_2O_2 and gases that may be found in ambient air. Typically, the reactivity of O_3 and NO_x (NO_2 and NO) was evaluated using gas generation (for O_3) and diluted standards (NO_2 and NO). In a second stage, ambient air under different conditions was assessed. A measurement campaign was carried out at a watchmaking factory where workers are exposed to oil mist, where off-line OP^{FOX} were taken simultaneously.

Blank measurements' daily variability did not exceed 30 %. The introduction of systematic blank measurements into the OP determination sequence will enable robust compensation of signal background. The liquid H_2O_2 calibration allowed expressing the OP as H_2O_2 equivalent, but a calibration using would be more accurate. The FOX assay reactivity to O_3 relative to liquid H_2O_2 is about 5 %, whereas it did not react to NO_x (NO and NO_2) in environmentally relevant concentration range. The OP measuring device prototype could detect environmental air quality changes, occurring due to the presence of a nearby construction site emitting PM. On-line and off-line measurements at the watchmaking factory bring some evidence that the gas and particulate fractions of the aerosol might contribute differently to OP.

In future work, the OP^{FOX} measuring device prototype will be further improved. The prototype reactivity to particles, as well as the influence of meteorological variables on the OP^{FOX}, will be assessed.

Keywords: ambient air / environmental oxidative potential (OP), FOX assay, PM, on-line measurement

Contents

List of Figures

List of Tables

1   Introduction

Outdoor air pollution is estimated to cause approximatively 4.2 million yearly premature deaths worldwide [1]. In Switzerland, atmospheric pollution by PM_{10} is estimated to causes 2300 yearly premature fatalities (the estimation was made for 2018) [2]. 14000 hospitalization days for cardiorespiratory or vascular diseases are attributed to (outdoor) air pollution in Switzerland per year [2, 3]. The health costs of atmospheric pollution in Switzerland are about 7 billion CHF per year [2]. Indoor pollution can also cause health problems [4, 5]. It is worth noting that indoor air pollutants concentrations can be 2 to 5 times higher indoors than outdoors [4]. Among the various health issues caused by air pollution, cardiorespiratory illnesses are of prime importance [6–8]: difficulty breathing, cough, sputum, chronic and non-chronic bronchitis, respiratory tract infection, [6], chronic obstructive pulmonary disease [9], lung cancer [4], etc.

Due to its important health and related economic impact, air pollution shall be monitored and regulated. In Switzerland, outdoor air pollution is regulated via the Ordinance on Air Pollution Control (OAPC) [10]. There is no comprehensive law text that regulates indoor air pollution in Switzerland [11], except for radon regulation in the Radiological Protection Ordinance (RPO) [11, 12], smoking ban in indoor public spaces and workspace used by several people [11, 13, 14], and product emission controls at the manufacturing stage [11].

Air pollution is typically measured as the mass concentration of air pollutants such as particulate matter (PM_{10} and $PM_{2.5}$), ozone (O_3), nitric oxide (NO), nitrogen dioxide (NO_2), etc. [7, 15]. Aggregated metrics, for instance, an air pollution index, are also used. More specifically, in Switzerland short and long-term air pollution indexes are used [16, 17]. They are built from mass concentration (in $\mu g/m^3$) of PM_{10}, O_3, and NO_2 [16, 17].

In the case of PM, the issue with the mass concentration metric is that it does not necessarily reflect the toxicological effect that PM can have. Particulate matter is composed of many different solid particles and liquid droplets [18]. Yet a small amount of a more toxic compound can have a larger impact than a bigger amount of a less toxic compound. Often low toxicity compounds make up the majority of the mass of PM [19]. Moreover, PM composition undergoes spatio-temporal variations [7]. In addition to the chemical composition of PM, the size of the particles matters [20]. Smaller particles are more likely to travel further down the respiratory tract than larger particles [20]. This is taken into account by indicating the size of the particles, PM_{10} particles corresponding to 50 % of the particle distribution having sizes smaller than 10 μm in diameters and $PM_{2.5}$ smaller than 2.5 μm.

The mechanisms of PM toxicity are not well known, although oxidative stress is believed to be one of them [7]. Oxidative stress happens when the body's antioxidants cannot counteract reactive oxygen species (ROS) because their concentration is too high, thus changing the redox state of cells [7]. It can "*initiate or exacerbate inflammation in the respiratory tract and cardiovascular systems, chemically alter DNA, proteins, and lipids, and lead to cell and tissue damage or death*" [7]. Reactive oxygen species, such as hydrogen peroxide (H_2O_2), superoxide radical ($\bullet O_2^-$), and hydroxyl radical ($\bullet OH$), are highly reactive molecules because they contain oxygen molecules with one or more unpaired electrons [7].

Given the above-mentioned limitations of mass concentration metrics for air pollution, an alternative metric is oxidative potential (OP) [7, 8]. OP reflects the capacity of air pollution to oxidize target probe molecules (exogenous ROS) which is linked to its ability to cause oxidative stress (endogenous ROS) [7, 8]. OP could be more convenient than traditional air pollution metrics (i.e., mass concen-

trations) because it directly reflects the potential of ambient air to cause oxidative stress. Moreover, epidemiological studies bring evidence that OP could be more correlated to health outcomes than PM mass [8]. Thus, some of the advantages of using OP over traditional mass concentration air pollution metric is that it would allow targeting air pollution mitigation measures to the sources that contribute the most to health effects and could influence spatial planning policies. Although OP would theoretically allow considering the ability of ambient air to cause oxidative stress, it should be noted that the aerosol gaseous fraction is often not considered, although it could substantially contribute to ambient OP [21, 22].

So far, there is no consensual OP measurement method [7, 8, 22]. Different OP assay react differently to different particle compositions, sources, photochemistry, and PM size distribution [8]. Some OP assays such as electron spin resonance (OP^{ESR}) or high-performance liquid chromatography (HPLC) measure ROS generation [8]. Other assays measure the depletion rate of proxies for antioxidants or reductants: ascorbic acid assay (OP^{AA}, antioxidants), glutathione assay (OP^{GSH}, antioxidant), and dithiothreitol assay (OP^{DTT}, reductant) [8].

Another way to measure the OP is based on the colorimetric FOX assay (Fe^{2+}/orange xylenol) [22–30]. The principle behind this assay is the oxidation of Fe^{2+} into Fe^{3+}, which then forms a complex with orange xylenol (OX) [22, 26–28]. This Fe^{3+}/OX complex shows an absorption peak at 580 nm, which can be measured by spectrometry [22, 26–28]. Sorbitol is added to the assay to increase its sensitivity via the generation of radical chain reactions [24, 26, 27]. The FOX assay presents the advantage of reacting to oxidants and reducing agents as the reaction between Fe^{3+} and orange xylenol is reversible [28]. Thus a positive OP value (expressed in H_2O_2 concentration equivalent) corresponds to an sample exhibiting oxidative behavior towards Fe^+ whereas a negative OP value means the analyzed sample acts as a reducer. [28].

Sauvain et al. used the FOX assay as an off-line measurement (filters were used to collect the media) to assess the professional exposure to aerosols of metalworking fluids (MWF) used during industrial metal cutting [22]. The advantage of measuring the OP instead of simply particle mass is that it focused on the hazardous fraction of oil mist [22]. Moreover, it allowed taking the gaseous fraction into account [22]. The authors found that the water-based MFA showed the greatest OP^{FOX} regarding the particulate fraction [22]. The oil mist gaseous fraction was non-negligible regarding its redox activity [22]. Thus OP^{FOX} seems a more relevant metric to assess MWF occupational exposure than particle mass [22].

However, off-line measurement methods present some disadvantages: the filter only collects the aerosol particulate fraction, the solvent used for the PM extraction from the filter as well as the filter type and storage time (for the DTT assay) influence the result, and storage issues may lead to an underestimated OP [31–34]. On-line measurement methods for OP could avoid these problems while reducing the time resolution of measurements [31]. Some semi-automated OP measurement prototypes based on the DTT assay have been built [31, 35–38]. However, their commercialization possibilities and use are reduced due to the multi-step reaction sequence [31, 34].

An on-line OP measuring device prototype based on the FOX assay and multi-scattering-enhanced absorbance (MEA) was developed at Unisanté-DSTE (*Département Santé au Travail et Environnement* Occupational and Environmental Health Department [26]. In prior OP sensing device, the MEA condition has been achieved by increasing the probability of a photon getting absorbed [28] by adding a cellulose membrane or glass fibers acting as a random medium in the glass optical cell [26]. The limit of detection is 9nM H_2O_2 equivalent [26]. A peristaltic pump allows the FOX assay to

circulate in a closed loop in the system [26]. An air sampling membrane pump diffuses air into the FOX solution [26]. Measurements are taken in real time, every 5 to 15 seconds thanks to a mini spectrometer [26]. The device was tested to measure reactive oxygen species (ROS) in traffic and exhaled breath as a lung inflammation biomarker on two healthy, non-smoker volunteers. [26]. The OP of traffic air was almost twice as high as the control air indoor [26]. The exhaled air presented a lower OP than the control air, possibly due to the presence of antioxidants in the pulmonary lining fluid, with a very small fraction known to be exhaled [26]. However, a larger sample would be necessary to draw significant conclusions [26].

In a subsequent study, this OP measuring device was used to assess the oxidation capacity of TiO_2 nanoparticles [27]. The authors found that UV light increases TiO_2 nanoparticles OP due to its photocatalytic activity under certain humidity conditions [27].

Another prototype using the FOX assay was built at Unisanté-DSTE and used to determine the oxidative potential in exhaled air (OPEA) of healthy subjects and patients affected by chronic obstructive pulmonary disease (COPD) [28]. In this prototype exhaled air is collected and injected into a 1 mL vial partly filled with FOX [28]. Measurements are taken thanks to a photosensor and optical cell in MEA conditions [28]. The comparative analysis of different optical configurations clearly showed that MEA enables improvement in sensitivity and limit of detection over standard spectrophotometers based on the Beer-Lambert configuration [28].

Another prototype specifically aimed at measuring ambient air OP based on the FOX assay has been developed at Unisanté-DTSE. Two EPFL Design Projects allowed to partly characterize and suggest improvements for the prototype [29, 30]. It is worth noting that the FOX solution circulated continuously in the prototype [29, 30]. In Caquot et al. the measured PO was related to various pollutants concentrations (O_3, NO_x, NO, NO_2, PM_{10}, $PM_{2.5}$, PM_1) and environmental variables (external temperature, radiation, humidity, pressure, weather station temperature) measured at a Direction General de l'Environnement (DGE) weather station (Plaines-du-Loup) [29]. However, only one measurement campaign could be done, limiting the significance of the results. Moreover, improvements in the way to collect the particles based on a particle collector [39] were discussed [29]. Clark et al. investigated the prototype reaction to liquid and gaseous H_2O_2 as well as O_3 in the laboratory [30]. The prototype reacted to all of them, although the results were not entirely consistent [30]. The authors also used the prototype in a weather station (DGE, Plaines-du-Loup, Lausanne [30]. The prototype response seemed to be correlated to pollutants levels, although it appeared to present an artifact (a sudden, inexplicable increase in its value after a certain time) [30]. After those Design Projects, a significant change was made to the operation mode of the device; the continuously circulating FOX was replaced by a four-phase protocol: i) filling the bubbling cell with FOX; ii) bubbling with air sample; iii) FOX circulation to sensing cell; iv) optical measurement.

The main goal of this master project is to use the OP^{FOX} measuring prototype already built at Unisanté to understand the reactivity of the FOX assay towards ambient gases and particulate matter. The prototype reaction to H_2O_2 (in liquid and gaseous form), O_3, NO, NO_2, and ambient air in different scenarios is investigated. The prototype is also tested in a large watchmaking factory facing the problem of workers' exposure to oil mist. Moreover, several improvements to the prototype were made in the first phase of the project.

2   Material and Methods

2.1   Colorimetric FOX II assay

The ferric orange xylenol (FOX) solution is prepared in the following way. For 100 mL of FOX solution, 10 mg ammonium iron(III) sulfate (Mohr's salt, Merck), 10 mg of orange xylenol tetrasodium salt (Merck), and 1820 mg D-sorbitol (Merck) are weighted in a weighting plastic basket. A 100 ml solution of 25 mM sulfuric acid (H_2SO_4) is prepared by diluting the 1 M sulphuric acid stock solution. The 25 mL sulphuric acid solution is used to dissolve the reagents. Part of the 25 mM H_2SO_4 solution is poured onto the mixture of Mohr's salt, orange xylenol, and sorbitol and mixed with a Pasteur pipette. The resulting liquid is poured into a bottle. The rest of the sulphuric acid solution is added to it. The FOX is used immediately after or conserved in a freezer until needed.

2.2   OP measuring device prototype

At the beginning of the project, an OP measuring device prototype was available. The initial OP measurement device prototype was progressively improved during the project. The corresponding modifications are described in detail in section 3.1. The experiments reported hereafter were made with an advanced version of the prototype because some experiments were not conclusive with the previous versions of the prototype. It is worth noting that the prototype is still being improved in the frame of the DIROP (*Testing of a direct reading instrument for oxidative potential measurement*) project (Federal Office for the Environment (FOEN) Environmental technology promotion).

The operation principles of the OP measuring device common to all versions of the prototypes are described hereafter. Figures 2.1 and 2.2 provide some illustrations of the OP measurement device. The numbers in the text hereafter refer to those of the figures mentioned above.

The FOX solution lies in a reservoir bottle ((1) fig. 2.1). A Teflon tube ((2) fig. 2.1) brings it into a bubbling cell ((3) fig. 2.1) through the action of a peristaltic pump (*P2*) ((4) fig. 2.2, 2.1)) during the *addition phase*. Then some air is bubbled into the FOX solution via a membrane pump (*P3*) at a flow of 111 ml/min for 1 min ((5) fig. 2.2). After the *bubbling phase*, the FOX solution is brought into the optical measurement cell ((6) fig 2.2)) via a second peristaltic pump (*P1*) ((7) fig 2.2, 2.1)). The measurement cell relies on MEA as described in prior article (Laulagnet et al. [26]) in which high reflecting optical cell coating (aluminium) ensures an efficient elongation of the optical path. The geometric dimensions of the optical cell (glass tube) are 117 mm length and 3 mm internal diameter. Two photosensors separated by 10 cm at the measurement cell extremities define the effective sensing volume. After this *circulation phase*, a *measurement phase* takes place, in which mixture FOX-sample remains static in the measurement cell. The sequence "addition, bubbling, circulation, and measurement" constitutes a cycle that is continuously repeated over the full measurement period. When new FOX circulates from the bubbling cell into the measurement cell, the FOX that was previously in the measurement cell is driven to the waste container ((8) fig. 2.1)). The measurement cell shall be in the dark so that the ambient light doesn't interfere with the measurement. Throughout the experiment, the absorbance is measured at 580 nm (sensing wavelength) and 700 nm (reference wavelength).
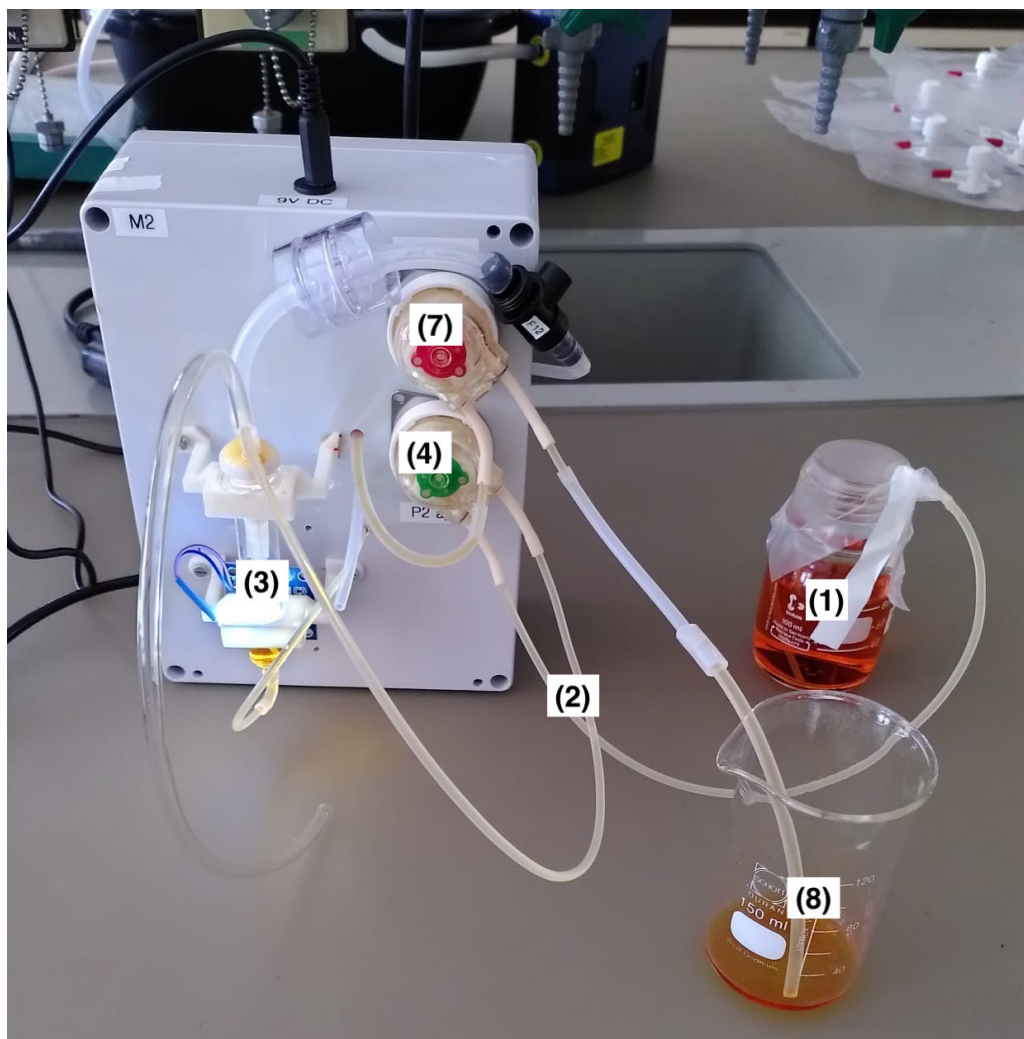
Figure 2.1: Picture of the OP$^{\text{FOX}}$ measuring device prototype (outer part)
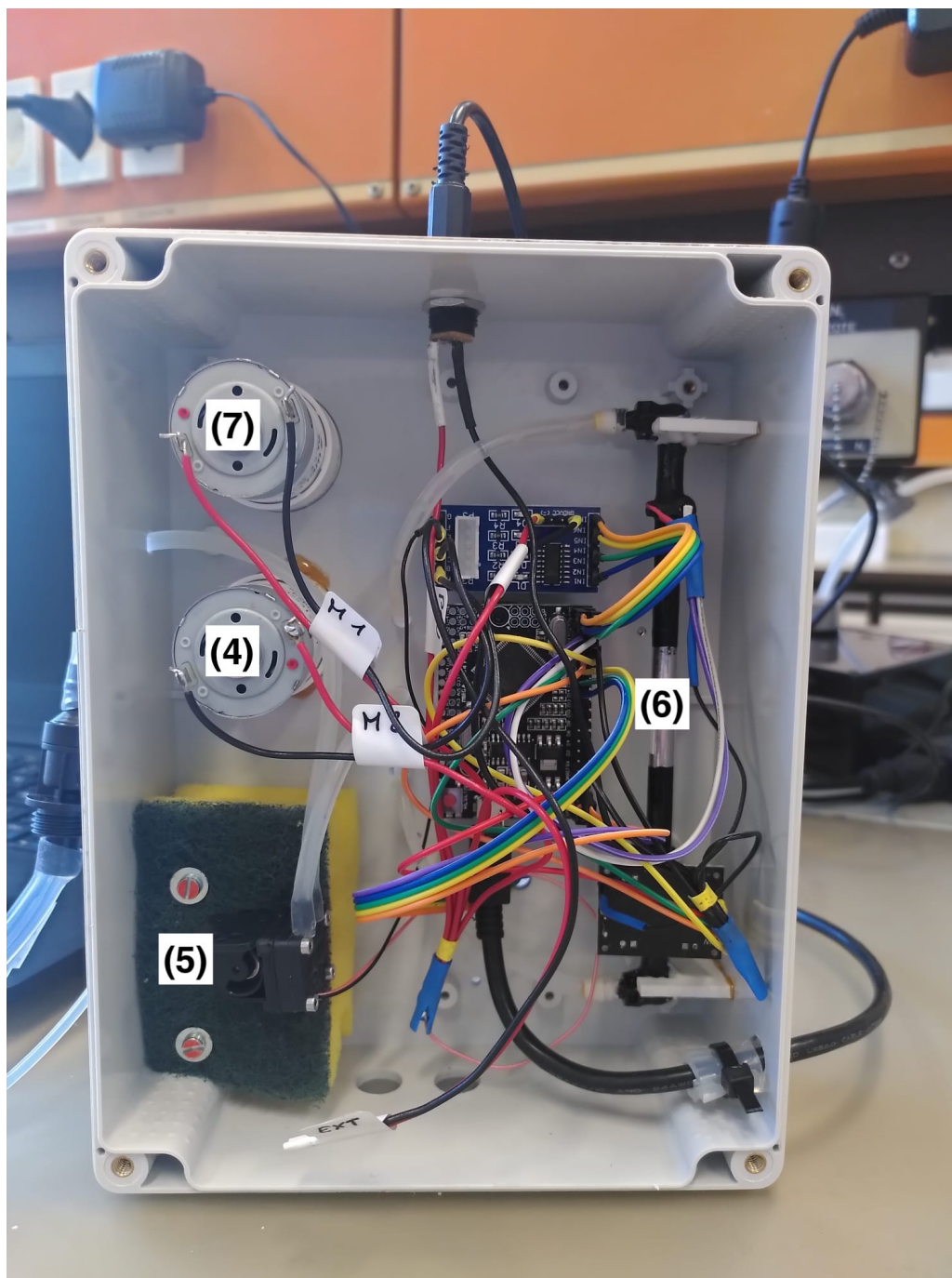
Figure 2.2: Picture of the OP$^{\mathrm{FOX}}$ measuring device prototype (inner part)

The automation of the device is achieved by a microcontroller (ATMEGA 32, Arduino). A CoolTerm interface (open source) allows controlling the machine during experiments by using various parameters, such as "p1", "p2", and "p3" to turn the peristaltic pumps P1, P2, and membrane pump P3 on and off. The parameter "on" starts a cycle (addition, bubbling, circulation, measurement). Setting the value of the corresponding parameters by typing their names followed by the desired value allows setting the duration time for each phase (addition, bubbling, circulation, measurement). It is possible to change the speed of the pumps similarly. The parameter "st" stops whatever pump is working at the moment. Section 3.1.2 lists other parameters added during the course of the project.

The serial terminal (CoolTerm interface) also prints various data every 5 seconds (see fig. 2.3),

such as the cumulative time since the interface was open, the number of measurements taken by the optic system in the 5 seconds, and the light intensity at 580 nm and 700 nm. It also provides a ratio of the light absorbances computed as follows:

$$\Gamma = \frac{A_{580}}{A_{700}} \tag{1}$$

Where A_i is the absorbance at wavelength i.

This data, the date, and the time are sent to a text file.
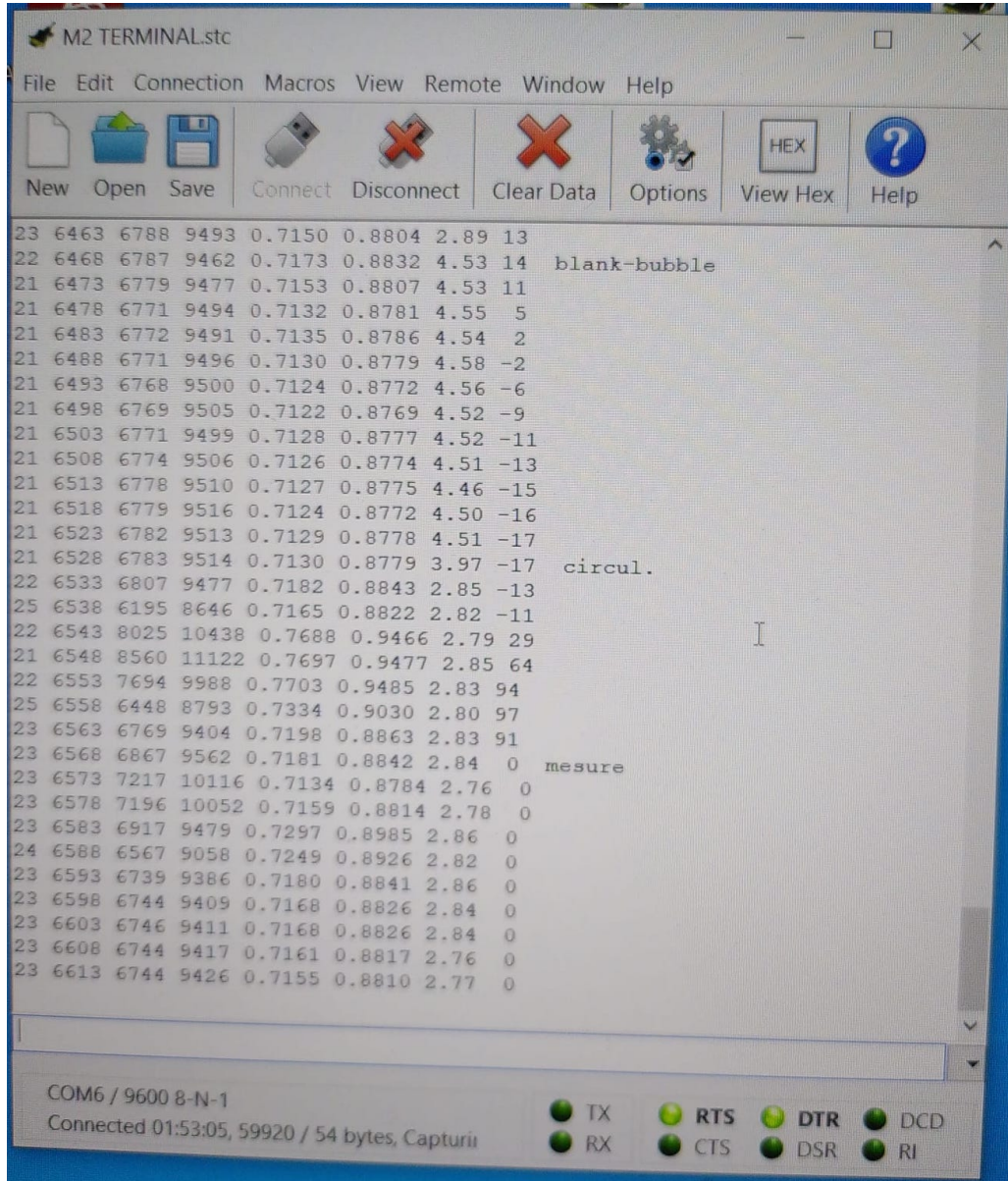
Figure 2.3: The Coolterm interface allows controlling the OP^{FOX} measuring device prototype. The interface also provides a series of data, for instance, the number of measurements taken by the optic system in the 5 seconds (column 1), the cumulative time since the interface was open (column 2), the light intensity at 580 nm (column 3) and 700 nm (column 4) and the ratio of the light absorbances (column 5). etc.

It is possible to insert a blank measurement after a certain number of cycles to assess the background

variation of the OP measuring device due to the FOX aging. In the current device version, the blank consists of the absence of bubbling step before the measurement. The frequency at which the blank occurs can be adjusted via the corresponding parameter ("bf") in the CoolTerm interface.

2.3   Expression of the OP

For all the experiments, the metric characterizing the OP is the slope of light intensity at 580 nm against the time from 65 to 150 seconds of the measurement time. The first minute of the measurement time is not included to allow the FOX reaction to reach steady-state conditions. The OP metric was computed with the Microsoft Excel function *SLOPE*. The original plan was to use the slope of the light intensity ratio, as the light intensity at 700 nm is supposed to act as a reference and correct the signal for instrumental variations (light intensity of the LED, electronic noise, presence of bubbles in the measurement cell, etc.). However, this correction didn't always work, probably because the infrared LED spectrum was too broad, allowing it to be influenced by FOX reaction, with an overlap of the corresponding emission and absorption spectra.

2.4   Blank

The FOX solution always reacts to some extent with oxygen when not stored at -20°C. In the prototype, the FOX is at ambient temperature. We observed that its absorbance at 580 nm is slightly increasing with time. In addition, a residue of FOX solution in the bubbling tank is also present (see fig. 2.4). Blanks would allow considering this background noise. Blanks were measured to take into account possible changes in the FOX absorbance over time. In this context, a blank consists of the absence of a bubbling step before the measurement. Eight experiments were done. Every experiment used the same FOX batch. It is worth noting that blanks are usually subtracted to measurement. However, it was not done in the experiments reported hereafter.
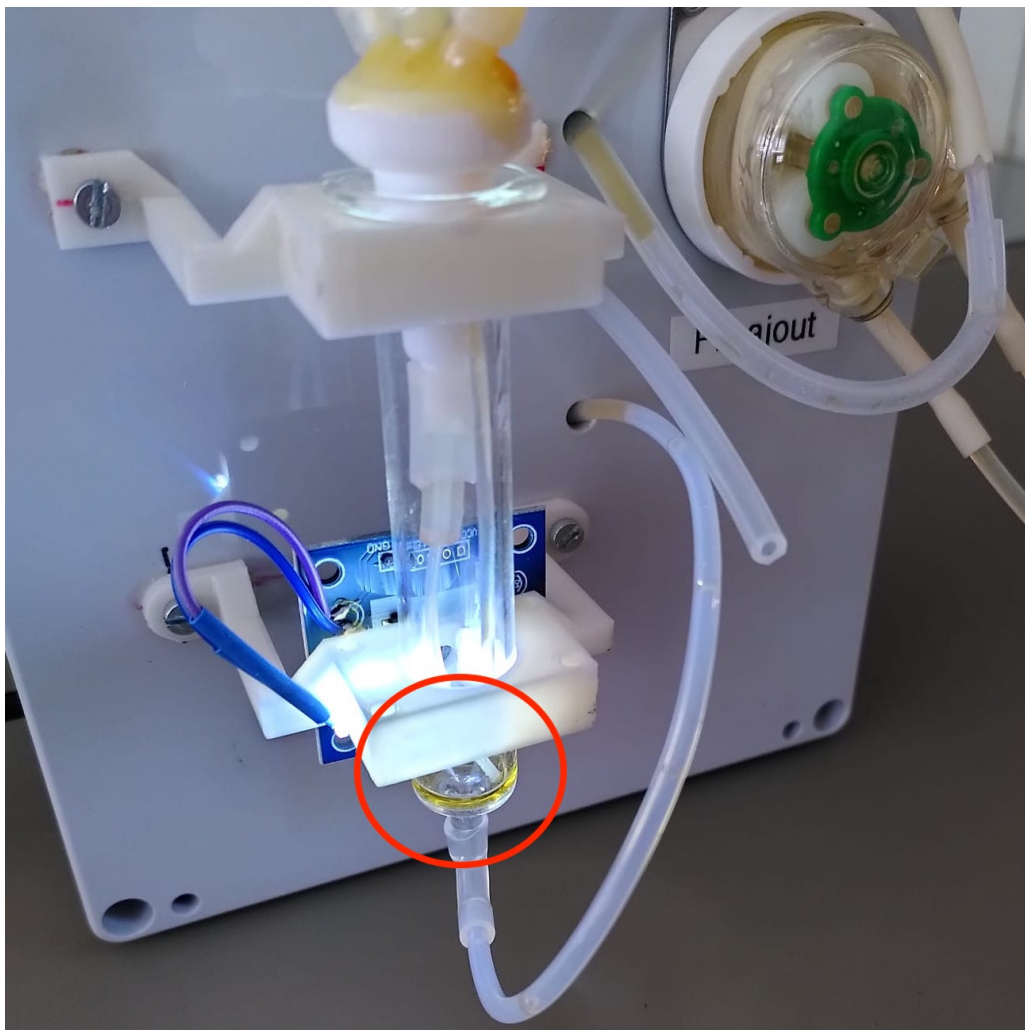
Figure 2.4: Residual FOX volume remains at the bottom of the measurement cell after the circulation phase.

2.5 H_2O_2 liquid calibration

The goal of this calibration is to assess how the FOX assay reacts to H_2O_2 in the liquid phase (the efficiency of the air-liquid interface achieved with bubbling does not play a role in this calibration) without adding the challenge of having to put H_2O_2 in the gas phase. The bubbling pump (*P3*) was disconnected. 10 μL H_2O_2 standard solution were directly added to the FOX solution in the bubbling cell and mixed using a pipette during the bubbling stage. The assessed concentrations were 0 M, 10^{-6} M, 10^{-5} M, 10^{-4} M in the first replicate and 0 M, 10^{-6} M, $2.5 \cdot 10^{-6}$ M, $5 \cdot 10^{-6}$ M, 10^{-5} M, $5 \cdot 10^{-5}$ M and 10^{-4} M in the second replicate. The standards were prepared from an 8 M H_2O_2 stock solution. D_2O ("heavy water") was used to dilute the stock solution to the relevant concentrations. Five replicates of each concentration per experiment were made. The measurement time was set to 150 seconds (2 minutes and a half). The bubbling phase (remember that P3 was disconnected) lasted 60 seconds. Blank measurements (nothing added to the FOX) were done between each addition of a new standard solution. They also took place at the beginning and the end of the experiment. The H_2O_2 dose D [mol] is computed as $D = C \cdot V$, where $C[M]$ is the H_2O_2 concentration and $V = 10$ μL is the H_2O_2 volume added.

2.6 H₂O₂ gaseous calibration

The H_2O_2 liquid calibration allowed assessing the FOX assay reactivity to H_2O_2 without the challenge of putting it into the gas phase. We hypothesize that H_2O_2 will partition between gas and particle in the ambient air. Therefore, a calibration with H_2O_2 in the gas phase was performed. An atomizer (Kesa electricals) evaporated 10 μL H_2O_2 standard solution ((1) fig. 2.5) at the beginning of the bubbling phase. The atomizer was connected to the OP measuring device pumping air tube ((2), fig. 2.5). It is worth noting that ambient air is bubbled in the FOX along H_2O_2 in the gas phase. The assessed concentrations were 0 M, 10^{-6} M, $2.5 \cdot 10^{-6}$ M, $5 \cdot 10^{-6}$ M, 10^{-5} M, $5 \cdot 10^{-5}$ M and 10^{-4} M. The standards were prepared from an 8 M H_2O_2 stock solution. D_2O ("heavy water") was used to dilute the stock solution to the relevant concentrations. Five replicates of each concentration were made. The measurement time was set to 150 seconds (2 minutes and a half). The bubbling phase lasted 60 seconds. Blank measurements (nothing added to the FOX) happened between the assessed concentration. They also took place at the beginning and the end of the experiment. Ambient air was bubbled before assessing gaseous H_2O_2. The H_2O_2 dose D $[mol]$ is computed as $D = C \cdot V$, where $C[M]$ is the H_2O_2 concentration and $V = 10$ μL is the the H_2O_2 volume added.
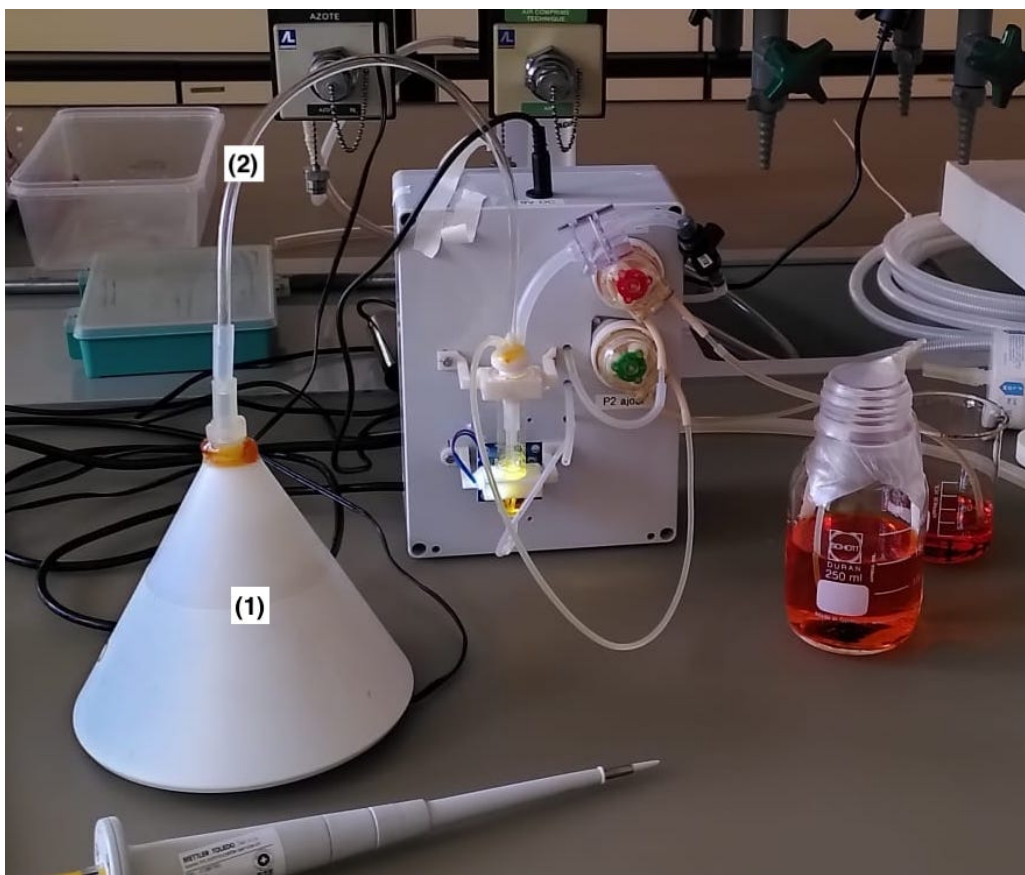
Figure 2.5: H_2O_2 gaseous calibration experimental setup

2.7 Determination of the range of environmentally relevant concentrations for O₃, NO₂ and NO

In order to test the prototype response to oxidant concentrations corresponding to ambient levels, data from the National Data from National Air Pollution Monitoring Network (NABEL) was used. It allowed determining the environmentally relevant range of concentration for O_3, NO_2 and NO in

Switzerland [40]. NABEL comprises 16 outdoor air pollution monitoring stations [41]. Those stations represent different location types: urban roadside, urban, suburban, rural motorway, rural under 1000 m.a.s.l, rural above 1000 m.a.s.l, and high alpine [42]. Hourly data of every location for the years 2018, 2019, 2020, and 2021 were used. As the measurement resolution of the OP measuring device is about five minutes, it makes more sense to use hourly data (the smallest resolution available here) than daily or monthly averages. Averaging over some time smoothes the data, not allowing to capture peaks. The data for 2022 is available but was set aside as it hasn't been verified yet. Potential measurement errors may still be present. Several recent years were used to get a representative picture of the concentrations. The software RStudio [43] was used to analyze the data. The data for NO was not available. However, NO_2 and NO_x levels were given. As NO_x is the sum of NO_2 and NO, the NO levels were deduced by subtracting the NO_2 concentrations to the NO_x ones. The overall maximum concentration (in $\mu g/m^3$) was computed for each pollutant and converted to *ppb* by using the following formula:

$$C[ppb] = C[\mu g/m^3] \cdot \frac{10^9 \cdot 10^{-6} \cdot RT}{MP} \tag{2}$$

where C is the concentration, 10^9 is a conversion factor, 10^{-6} is a conversion factor from μg to g, $R = 8.206 \cdot 10^{-5}$ $[m^3 \cdot atm \cdot mol^{-1} \cdot K^{-1}]$ is the perfect gas constant, $T = 293.15$ $[K]$ is the temperature, M $[g \cdot mol^{-1}]$ is the molar mass of the considered gas, and $P = 1$ atm is the ambient atmospheric pressure.

2.8 O_3 calibration

Figure 2.6 shows the experimental setup used to evaluate the reactivity of O_3 towards the FOX assay. O_3 was generated in a 10 m^3 cabin ((1) fig. 2.6) using an O_3 generator (built at Unisanté-DSTE) ((2) fig. 2.6). A ventilator ((3) fig. 2.6) was used to mix the air in the cabin (a homogeneous ozone concentration can be assumed). An O_3 concentration measuring device (aeroqual series 500, (4) fig. 2.6) was used to monitor the O_3 concentration in the cabin. The concentration was increased up to around 150 ppb (the maximum ozone level before risking damaging the O_3 concentration measuring device). Then the O_3 generator was switched off. The O_3 concentration was still recorded while decreasing. In the end, the remaining ozone was dispelled using ventilation. All along, the OP measuring device ((5) fig. 2.6) took measurements. A tube ((6) fig. 2.6) allowed retrieving air from inside the cabin. The bubbling phase lasted for 60 seconds. The measurement lasted 150 seconds (2 minutes and a half). A blank measurement happened every five cycles (i.e., four measurements for which air was bubbled into the FOX, followed by a blank). The O_3 concentration at the time of bubbling was related to the measured signal and deriving slope. The O_3 dose D_{O_3} $[mol]$ introduced in the bubbling tank is computed as $D_{O_3} = C_{O_3} \cdot Q \cdot t / M_{O_3}$, where C_{O_3} $[\mu g/m^3]$ is the O_3 concentration, $Q = 1.11 \cdot 10^{-4}$ $m^3 \cdot min^{-1}$ is the rate of air pumped, $t = 60$ min is the bubbling time and $M_{O_3} = 48$ $g \cdot mol^{-1}$ is the ozone molar mass. The concentration in ppb is converted in $\mu g/m^3$ using the inverse of equation 2.
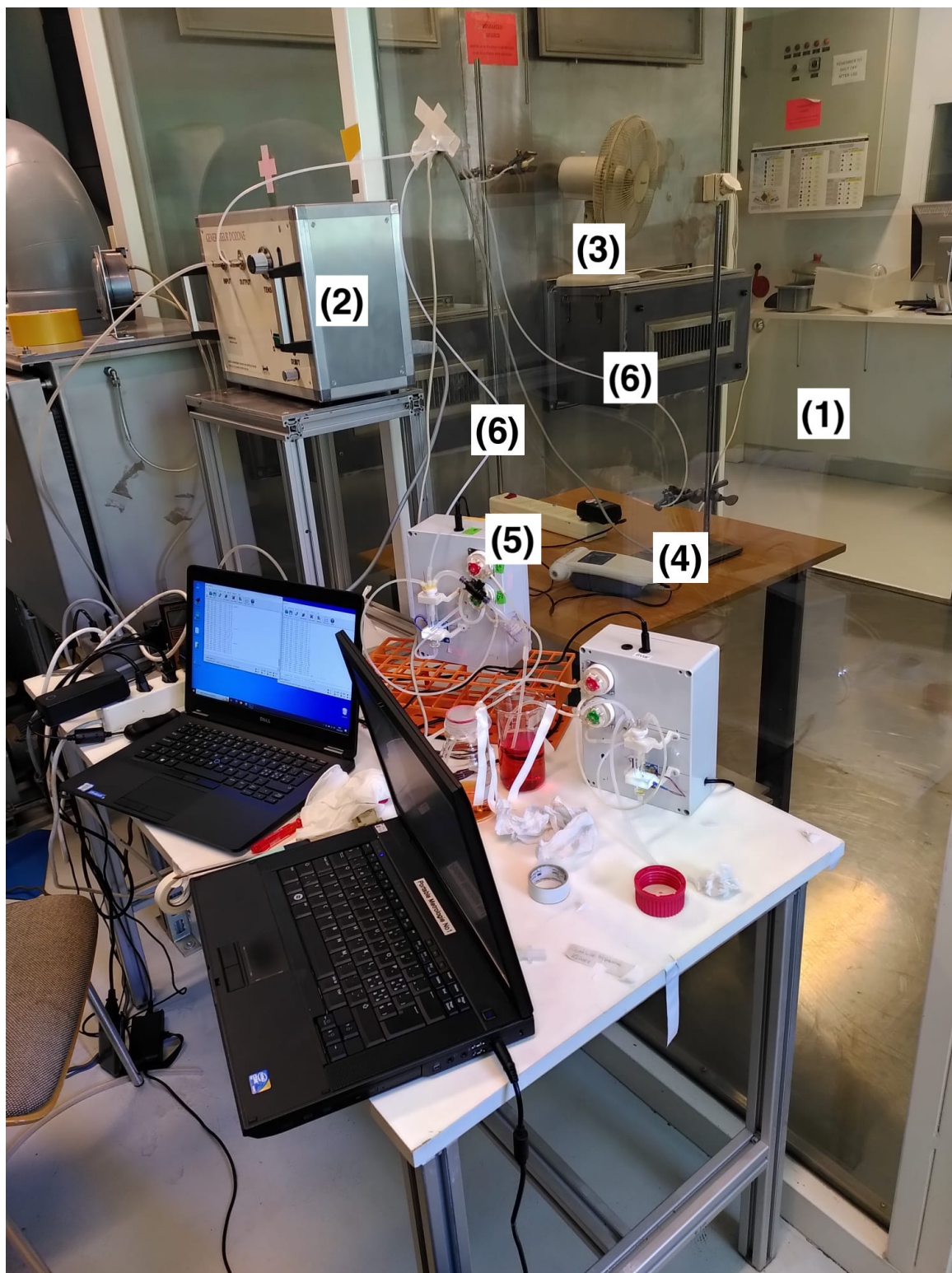
Figure 2.6: Experimental setup to assess the reactivity of O_3 towards the FOX assay

2.9 NO₂ calibration

NO$_2$ at 20 ppm in a gas cylinder (5 Litres, 150 bar in 20% O$_2$, 80% N$_2$) was diluted to obtain the desired concentrations. Some NO$_2$ at 20 ppm was transferred from the gas cylinder into a 1L Tedlar bag (Supelco, Merck). The dilutions were performed by filling another Tedlar bag with a known volume (approximately 1L) of technical-grade laboratory air. The appropriate volume of NO$_2$ was then taken

from the first Tedlar bag with a syringe and injected the into the other Tedlar bags filled with 1 L technical-grade laboratory air. The Tedlar bags ((1) fig. 2.7) were connected to the OP measuring device. The following concentrations were tested: 0 ppb (technical lab air), 30 ppb, 50 ppb, 100 ppb, and 200 ppb (first experiment); 0 ppb, 100 ppb, and 200 ppb (second experiment); 0 ppb and 200 ppb (third experiment). An explanation of the chosen concentrations can be found in the discussion (see subsection 3.7). For each experiment, five replicates of the assessed concentrations were carried out (except for the measurement of 0 ppb of the last experiment, where only four measurements were taken). A blank measurement was done between each tested concentration. Blank measurements were also taken at the beginning and end of the third experiment. Ambient air was assessed before NO_2 in the first and second experiments. The amount of NO_2 bubbled in the FOX for each measurement (the NO_2 dose) D_{NO_2} $[mol]$ is computed as $D_{NO_2} = C_{NO_2} \cdot Q \cdot t / M_{NO_2}$, where C_{NO_2} $[\mu g/m^3]$ is the NO_2 concentration, $Q = 1.11 \cdot 10^{-4}$ $m^3 \cdot min^{-1}$ is the rate of air pumped, and $t = 60$ s is the bubbling time and $M_{NO_2} = 46$ $g \cdot mol^{-1}$ is the NO_2 molar mass. The concentration in ppb is converted in $\mu g/m^3$ using the inverse of equation 2.
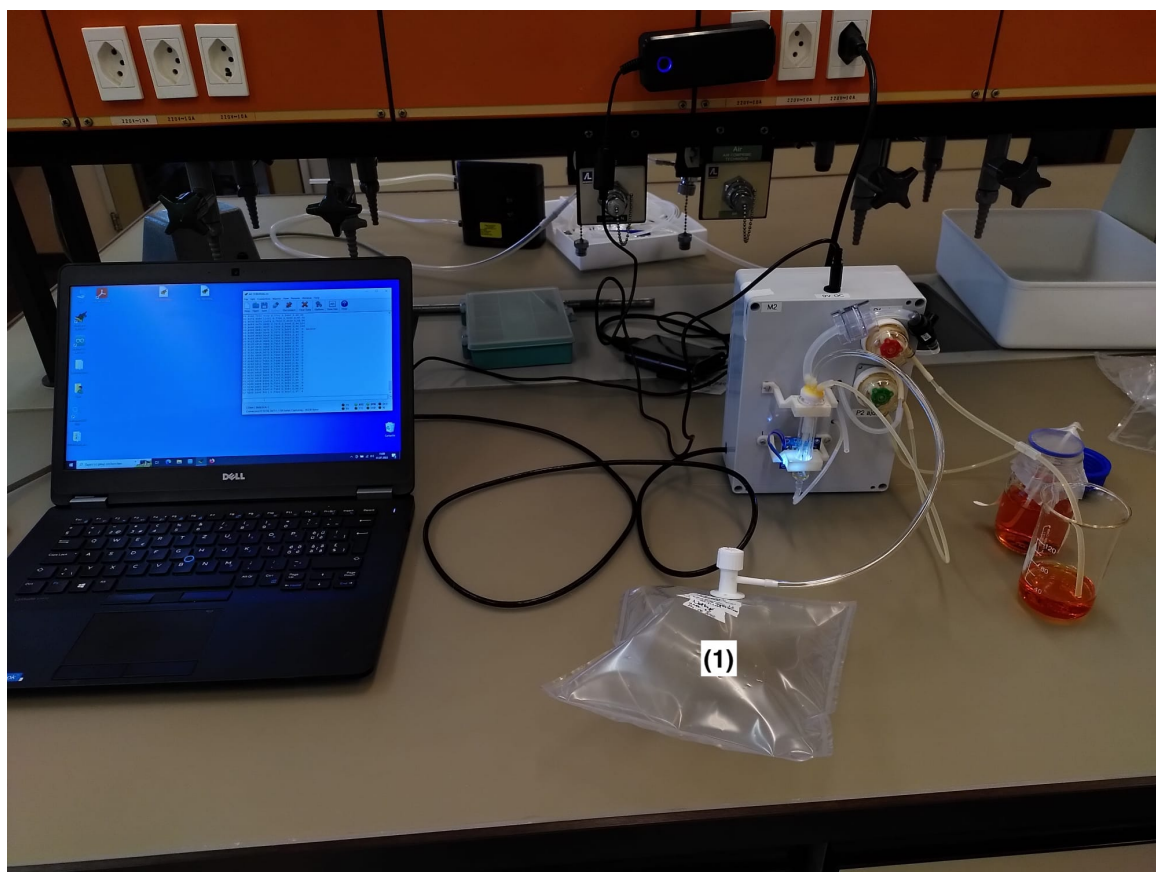
Figure 2.7: Experimental setup to assess the reactivity of NO_2 towards the FOX assay

2.10   NO calibration

NO at 20 ppm in a gas cylinder (5 Litres, 150 bar in 100% N_2, Carbagas) was diluted to obtain the desired concentrations. Some NO at 20 ppm was transferred from the gas cylinder into a 1 L Tedlar bag (Supelco, Merck). The dilutions were performed by filling another Tedlar bag with a known volume (approximately 1L) of N_2. The appropriate volume of NO was then taken from the first Tedlar bag with a syringe and injected the into the other Tedlar bags filled with 1 L N_2. N_2 is

used for the dilutions because it is an inert gas. Technical-grade laboratory air is not used to avoid NO converting to NO_2. The Tedlar bags were connected to the OP measuring device. The following concentrations were tested: 0 ppb (N_2), 200 ppb, 400 ppb, 500 ppb. Two replicates were carried out. For each experiment, five replicates of the assessed concentrations were carried out, except for the measurement of 0 ppb in both experiments (8 replicates) and the measurement of 500 ppb in the first experiment (3 replicates). A blank measurement was done between each tested concentration. Blank measurements were also taken at the beginning of both experiment replicates and the end of the second replicate. The amount of NO bubbled in the FOX for each measurement (the NO dose) D_{NO} $[mol]$ is computed as $D_{NO} = C_{NO} \cdot Q \cdot t/M_{NO}$, where C_{NO} $[\mu g/m^3]$ is the NO concentration, $Q = 1.11 \cdot 10^{-4}$ $m^3 \cdot min^{-1}$ is the rate of air pumped, and $t = 60$ s is the bubbling time and $M_{NO} = 30$ $g \cdot mol^{-1}$ is the NO molar mass. The concentration in ppb is converted in $\mu g/m^3$ using the inverse of equation 2.

## 2.11 Testing the OP measuring device prototype in ambient air conditions

The OP^{FOX} measuring device was tested for indoor and outdoor air. The experiment's first goal was to get an idea of the range of ambient air values obtained by the measuring device. The second goal was to assess whether the FOX assay is sensitive enough to detect changes like opening a window (fresh air supply; sometimes in the proximity of construction works) and filtering the air with a high-efficiency particulate air (HEPA) filter.

Indoor air was directly bubbled into the FOX solution. A 1 L syringe was used to collect outdoor air, which was stored in a Tedlar bag. The bag was connected to the OP measuring device (as in the experiment with NO and NO_2). The experiment assessed the following air conditions: outdoor air next to a road (in Lausanne, in front of the metro stop $CHUV$), indoor laboratory air (window closed), indoor laboratory air with an open window next to building works, and indoor laboratory air with a HEPA filter (closed window).

2.12 Testing the OP measuring device prototype in an occupational health context

The OP measuring device took measurements at a watchmaking company where workers were exposed to oil mist. The measurements were done under normal working activities. Two locations were assessed in the room: one sampling site on the "south" side of the atelier, nearby a new CNC starting its production, and the second on the "north" side of the atelier, where CNCs have been operating for a long time. The "south" location is expected to have a higher oil mist concentration, as mentioned by the responsible for the atelier. Gravimetry, volatile compounds, OP^{FOX} (off-line sampling and on-line measurements done by the prototype) measurements were taken simultaneously. On-line OP^{FOX} measurements on the north side of the atelier were done first without and then with a HEPA filer. The off-line OP^{FOX} measurement consisted in filtering air through an IOM head (inhalable fraction) equipped with a tefloned glass fiber filter (25 mm, EMFAB TX40H120, Pall LifeSciences) and a sampling pump set at 2 $L \cdot min^{-1}$. After a gravimetric measurement, the OP^{FOX} was determined by cutting the filter into small pieces of known surface and introducing them in vials containing 1 ml FOX. The vials were shaken for 1 min with a stirrer and then inserted into an off-line measurement device built at Unisanté-DSTE. The absorbance at 580 nm was measured for six minutes in triplicate. The first minute was excluded when computing the slope of the absorbance at 580 nm versus time. The OP FOX offline measurement device was calibrated by putting 100 μL H_2O_2 standards ranging

from 0 to 5 nM in 1 mL FOX.

2.13   Data analysis

The software RStudio was used for the subsequent analysis and to produce the graphs.

A calibration curve was done by plotting the slope of the absorbance measured at 580 nm as a function of the amount of liquid H_2O_2 introduced into the FOX solution. For the gaseous H_2O_2 test, it was not possible to obtain a calibration curve. The response of the prototype to O_3 was evaluated by plotting the H_2O_2 equivalent amount in the bubbling cell (using the calibration curve) as a function of the amount of O_3 in the air.

Regarding NO_2 and NO, the tested samples are assessed using boxplots [44], as calibration curves could not be established. Moreover, a Mann-Whitney U test (also called a Mann–Whitney–Wilcoxon test) is performed to assess whether each sample distribution differs or not from the 0 pmol sample distribution. The null and alternative hypothesis are as follow:

H_0: The distributions are identical
H_1: The distributions are different

The p-value is used to decide whether to reject H_0 or not. The p-value is defined as the smallest significance level α at which the null hypothesis H_0 is rejected. So if the p-value is smaller than the chosen confidence-level alpha, the null hypothesis is rejected. Otherwise, it is not rejected. A significance level of $\alpha = 0.05$ is used. The R function *wilcox.test()* is used.

The results regarding ambient air and the watchmaking factory are also given as boxplots. Mann-Whitney-U tests are also performed to assess whether the differences between the different types of air are significant.

For the experiment with liquid H_2O_2, the OP is given as the slope of the absorbance at 580 nm as a function of the time (from one minute to two and a half minutes). For every other experiment, the OP is given as H_2O_2 eq. The absorbance slope at 580 nm is converted to H_2O_2 eq. using the liquid H_2O_2 regression equation.

Limits of detection (LOD) and quantification (LOQ) were computed for liquid and gaseous H_2O_2, O_3, NO_2, and NO using the formulas:

$$LOD_{OP} = 3 \cdot Std(Blank\ [0\ pmol]) \tag{3}$$

$$LOQ_{OP} = 10 \cdot Std(Blank\ [0\ pmol]) \tag{4}$$

Std stands for standard deviation. For liquid H_2O_2, the blank corresponds to the sample containing 0 *pmol* of the analyte of interest. However, there is a subtlety for O_3. In fact, due to the experiment protocol, there is no repetition of a 0 *pmol* sample measure. The standard error of the intercept for the linear regression is used instead of a standard deviation of multiple blank measurements. The standard error of the intercept is computed using the R function *lm()*. Concerning liquid H_2O_2 and O_3, *LOD* and *LOQ* are computed by dividing LOD_{OP} and LOQ_{OP} by the respective regression equation slope. Regarding gaseous H_2O_2, NO_2, and NO, *LOD* and *LOQ* were not computed, as no calibration curve could be established.

3   Results and Discussion

3.1   Improvements on the OP measuring device prototype and CoolTerm interface

3.1.1   Improvements on the OP measuring device prototype

One of the peristaltic pump was replaced to have two pumps with the same flow rate. It also allows faster FOX addition to the bubbling cell and circulation from the bubbling cell to the measurement cell by changing the electric power supply from 6 to 9 V direct current (DC).

In the initial version of the prototype, the FOX height in the bubbling cell was controlled by the time of the addition phase. However, the accuracy of the settings (1 second) did not allow for enough precision. Over time, the lack of precision could lead to too much excess or scarcity of FOX in the bubbling cell. Therefore, a level detector based on a LED light system was added to automatically control the FOX height in the bubbling cell. A mini LED source and a RGB photodetector ((1), fig. 3.1) are positioned at the height that the FOX is supposed to reach in the bubbling cell. When FOX in the bubbling cell reaches the photodetector level, a recorded signal reaches a threshold that triggers the pump *P2* to stop.
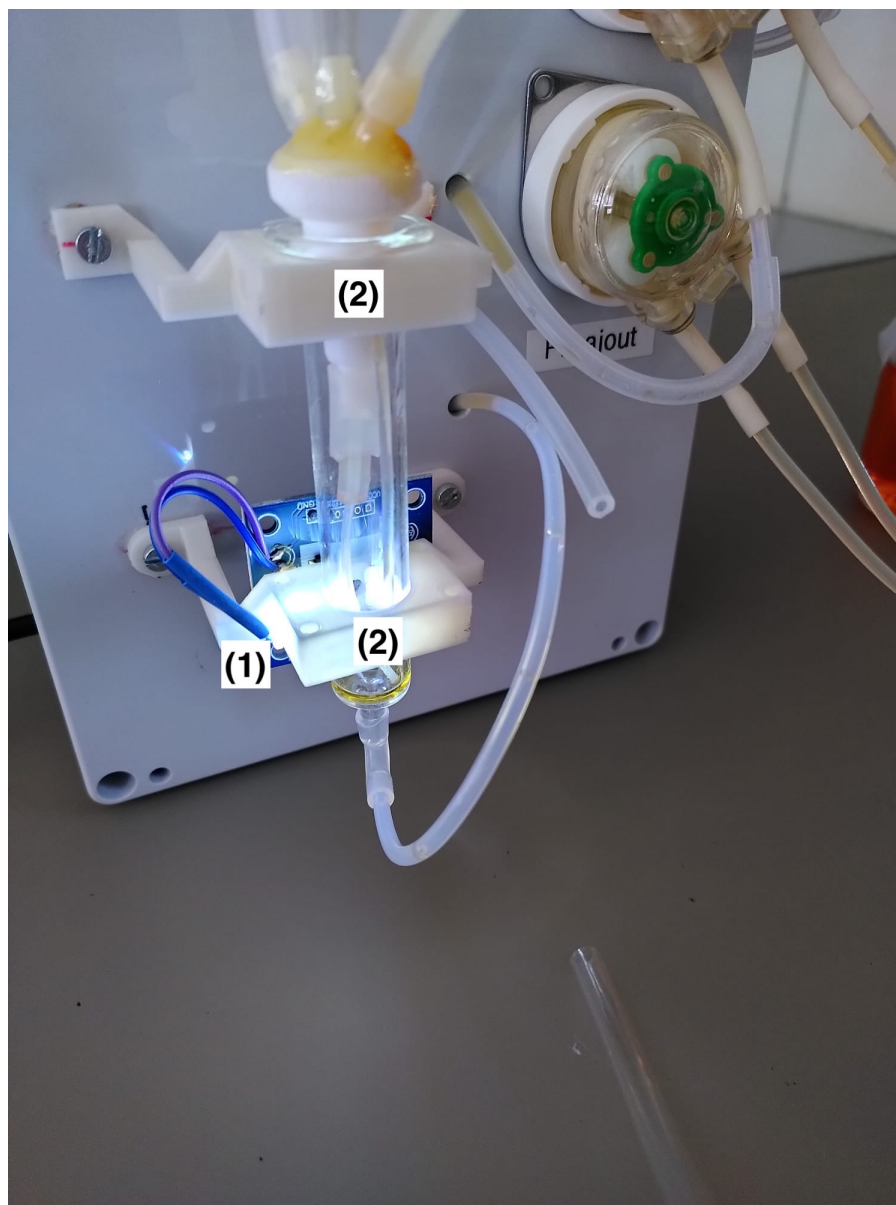
Figure 3.1: The LED/photodetector couple allowing control of the FOX level in the bubbling cell, and the new 3D printed piece holding the bubbling cell and LED system

The LED system and bubbling cells were attached to the device with specially designed 3D printed pieces ((2), fig. 3.1, to be compared with the old design image ((1), fig. 3.2).
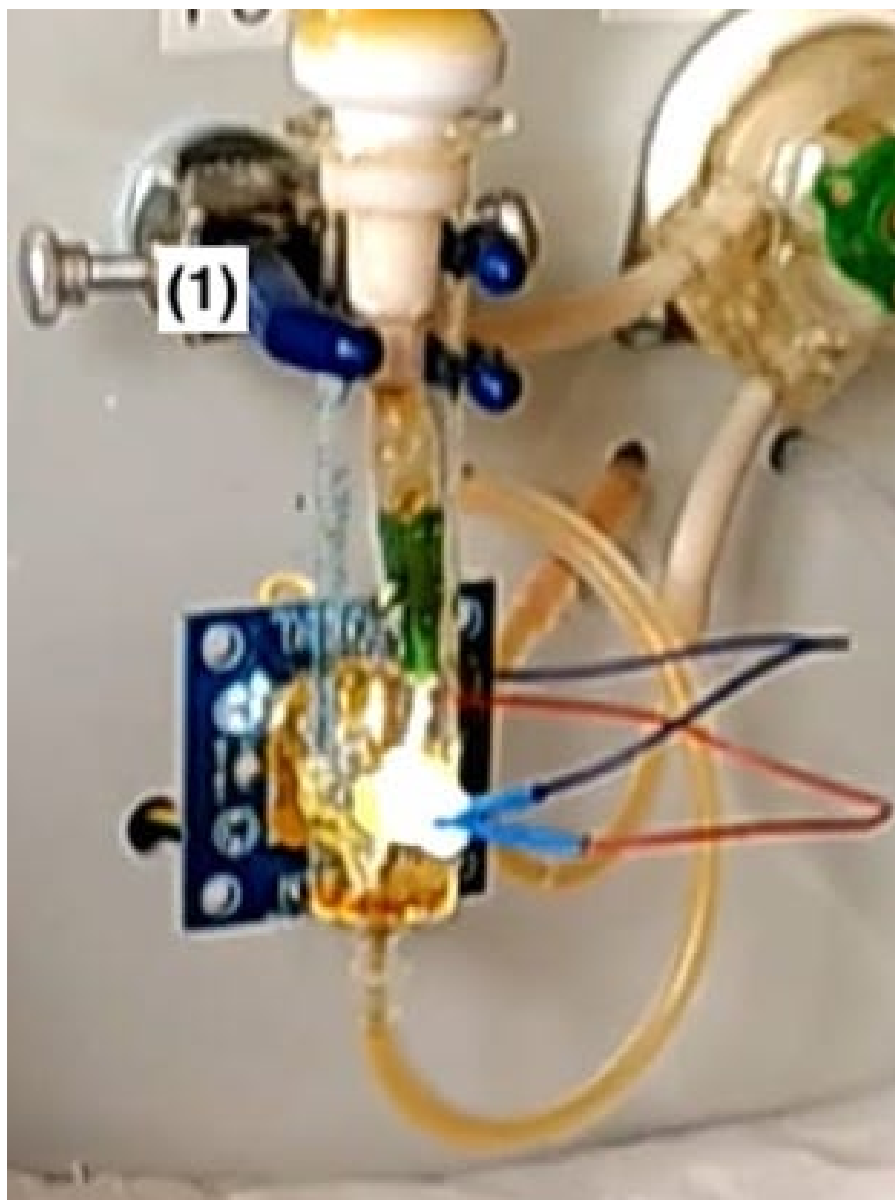
Figure 3.2: The old piece holding the bubbling cell

Most silicon tubes were replaced by Teflon^{TM} tubes to avoid FOX reacting with and adhering to the tubing system. Teflon^{TM} is an inert, anti-adhesive material.

Early into the project, it was noted that FOX was eventually ejected into the tube connecting to the air pump (*P3*) during the bubbling phase. Two measures were taken to avoid FOX reaching and damaging the air pump. First, a filter ((1), fig. 3.3) was set up to trap FOX that would go into the tube leading to the air pump. Then a valve ((2), fig. 3.3) was installed to control the air flux being bubbled into the FOX to avoid too big bubbles of air and thus FOX being ejected into the tube leading to the air pump.
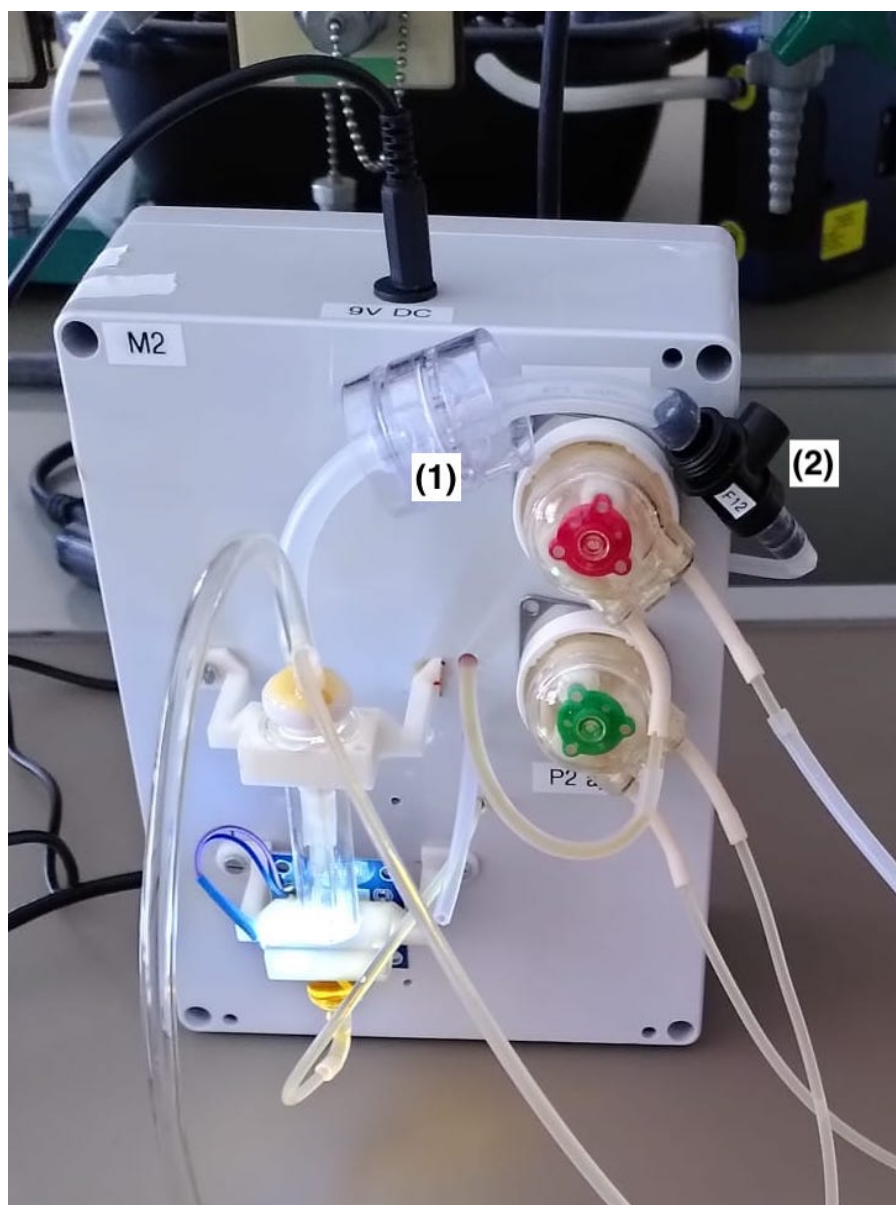
Figure 3.3: The filter protecting the air pump from the FOX, and the valve allowing control of the bubbling flow

At first, the measuring cell was laid horizontally. Its position changed to vertical to avoid stagnant air bubbles in the measurement cell.

The photodetector in the measurement cell was painted black to ensure no external light contamination.

The improvements cited above correspond to the OP^{FOX} measuring device prototype version used for the experiments reported hereafter.

Further improvements are underway. The team designed a new bubbling cell in ABS resin (Prima Creator) ((1) fig. 3.4) and a piece ((2) fig. 3.4) to hold it. A 3D printer allows the creation of these new elements. The new bubbling cell prevents FOX residual volumes to remain at the bottom of the cell. The bubbling cell walls have to be passivated as FOX was observed to oxidize quite rapidly without surface treatment. For that purpose, $NaBH_4$ (Sigma-Aldrich) was used to remove free radicals formed during printing. The $NaBH_4$ optimal treatment parameters ($NaBH_4$ concentration, exposure time, etc.) are to be determined. The tubes bringing FOX and air into the bubbling cell are integrated

inside the bubbling cell walls. The air tubes outlet are not exactly perpendicular to the bubbling cell walls. It allows creating a vortex to increase the air bubbles' residency time in the FOX and thus better mix the impinged air and the FOX. The filter protecting the air pump and the valve allowing to control the bubbling are now located directly at the air pump inlet ((3) fig. 3.4. Note that the filter is not shown here). The addition of a valve ((4) fig. 3.4) allows switching the air inlet. There is a filter at one of the inlets. It could allow filtering out particles and measuring the OP's gas fraction. Moreover, activated carbon could capture organics. Air without particles and organic compounds could serve as a blank (to be subtracted from the measurement).
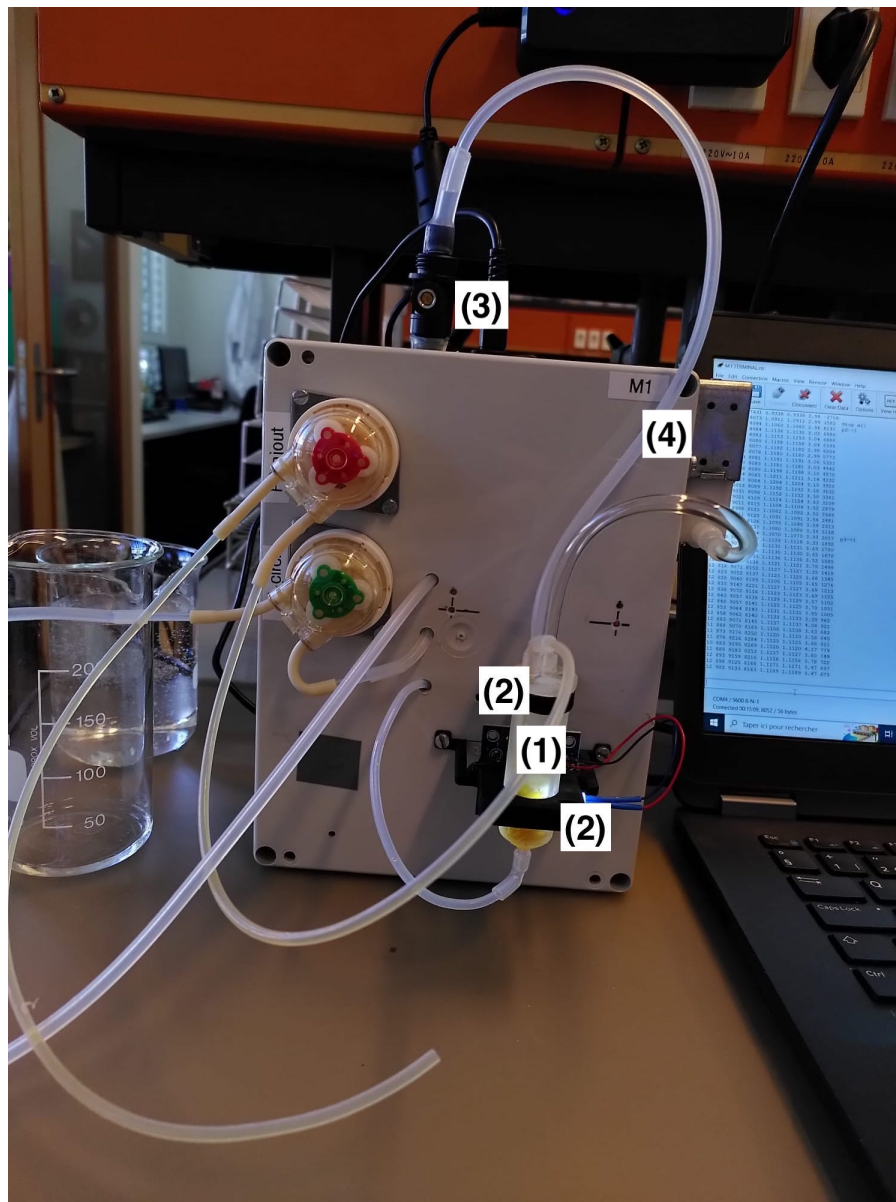
Figure 3.4: The newest OP$^{\text{FOX}}$ measuring device prototype version. Note that the filter protecting the air pump is missing. It should be on top of the valve controlling the air bubbling flow.

3.1.2 Improvements on the CoolTerm interface

The parameters adding time (t_a), bubbling time (t_b), circulation time (t_c), and measurement time (t_m) were can now be set with a finer 1 second step. At the beginning of the project, their values could only be a multiple of five.

The possibility was added to know the current value of one parameter by typing its name in the CoolTerm Interface.

Comments can be printed in the CooTerm interface thanks to a command called *co*. It is convenient to keep track of experiments unfolding. It can complement a laboratory notebook.

The possibility to insert a "*Blank Bubble*" was added. A *Blank Bubble* corresponds to a cycle during which a fresh FOX solution is introduced in the cell, but without further bubbling. It allows for evaluating the FOX aging and could act as a blank that could be subtracted from the measurement. The most appropriate way to carry out a blank measurement is still under discussion. The air without particles and organics mentioned above seems a good option. It has to be evaluated. The frequency at which a *Blank Bubble* occurs can be set thanks to the newly added parameter *bf* (blank frequency).

An algorithm computing the absorbance ratio (I_{580}/A_{700}) versus the time slope was implemented. The algorithm was written at a time when the OP metric *absorbance ratio slope* seemed to give promising results. However, it could easily be adapted to the other OP metric *slope of absorbance at 580 nm*.

3.1.3 Improvements on the measurement protocol

The importance of fully emptying the bubbling cell and its exit tubing between each measurement, was evidenced. It allows avoiding the FOX from a previous measurement to mix by diffusion with the new FOX. It also allows checking that only fresh FOX is present in the measurement cell. Fig. 3.5 illustrates the air bubbles between each measurement FOX.
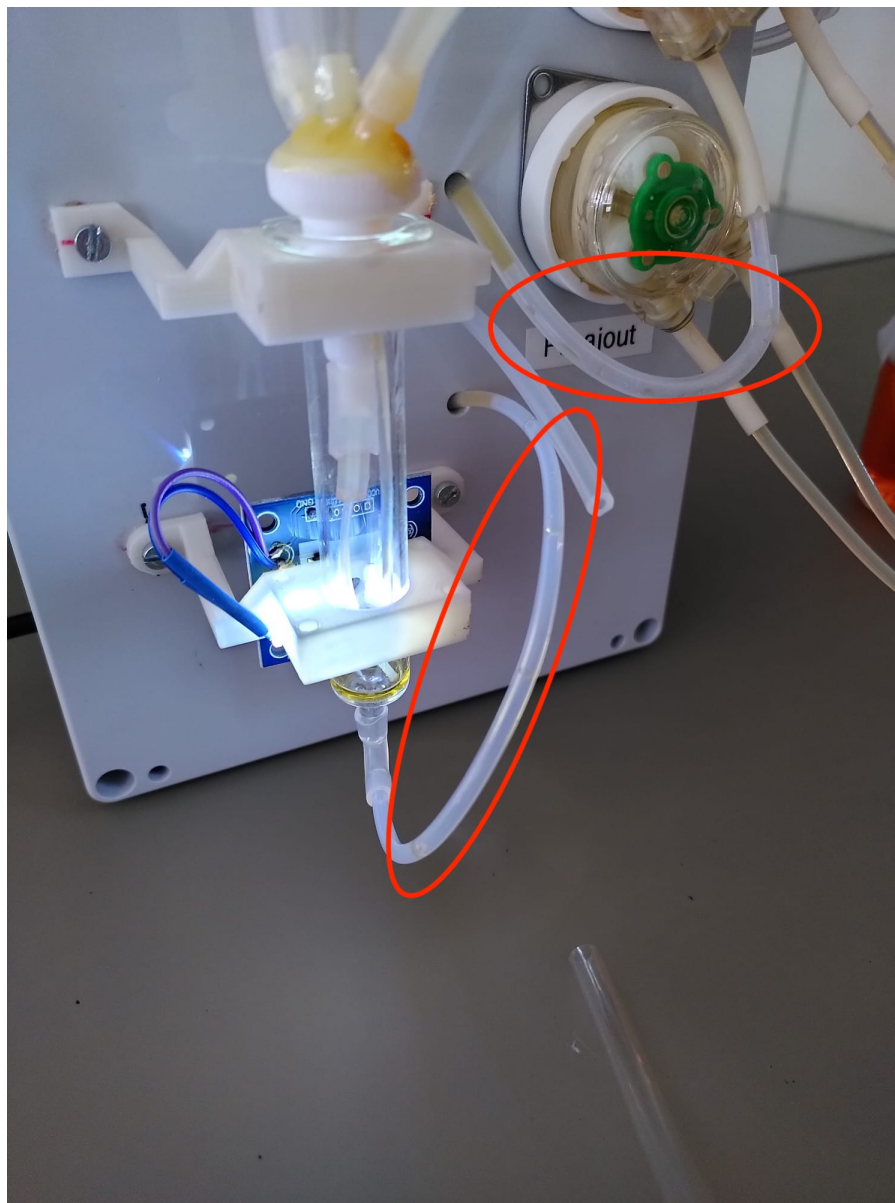
Figure 3.5: Air bubbles (circled in red) are left between each measurement FOX.

3.2 Blank

The results for the blanks (corresponding here to *Blank Bubbles*) are presented in fig. 3.6.
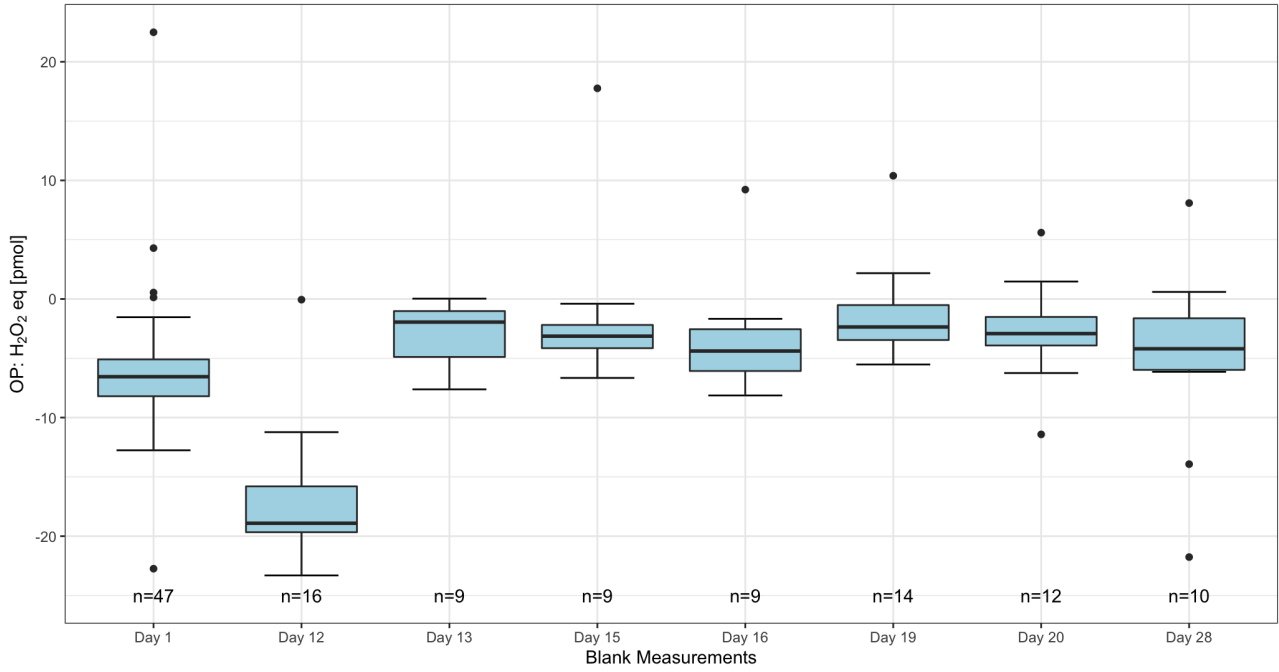
Figure 3.6: The blank measurement results. The days are counted from the day FOX was prepared.

The blank measurement distributions do not seem to differ, apart from the one on day 12 (see fig. 3.6). The Mann-Whitney U test brings some nuances to this hypothesis (see table 1).

Table 1: p-values and test interpretation for each blank measurement day relative to the day the FOX was prepared (day 1). The table upper half shows the p-values for each assessed pair. The table lower half shows whether H_0 is rejected at $\alpha = 0.05$ for each assessed pair.

	Day 1	Day 12	Day 13	Day 15	Day 16	Day 19	Day 20	Day 28
Day 1	-	4.9e-07	0.0079	0.0049	0.073	3.4e-05	0.0030	0.13
Day 12	Yes	-	6.6e-05	6.6e-05	6.6e-05	2.9e-05	6.4e-06	0.0012
Day 13	Yes	Yes	-	0.80	0.44	0.34	1	0.55
Day 15	Yes	Yes	No	-	0.49	0.36	0.60	0.45
Day 16	No	Yes	No	No	-	0.089	0.55	1
Day 19	Yes	Yes	No	No	No	-	0.70	0.095
Day 20	Yes	Yes	No	No	No	No	-	0.31
Day 28	No	Yes	No	No	No	No	No	-

The blank measurements on day 12 differ significantly from every other one. No explanation was found for this fact. From day 13 onward, the blanks are not significantly different. Day 1 blank measurement differ significantly from most following days (except day 16 and 28). It could be explained by FOX aging. However, it seems unlikely as FOX was stored in a freezer. In addition, the difference between days 13 and 28 as well as 1 and 28 is not statistically significant, although some days have passed. More likely explanations would be that the blank measurement depends on the time since the FOX was unfrozen and its temperature. These hypotheses should be tested with further experiments. The new bubbling cell form, in which FOX does not stagnates, will probably improve the quality of the results.

The measurement's variability for each day with all measurements is presented in table 2. The variability without the first measurement is also given because the first measurement seems to differ from the other ones most of the time.

Table 2: Blank variability for each measurement day, with every measurement and without the first one.

	Variability with every measurements [%]	Variability without the first measurement [%]
Day 1	19.20	13.55
Day 12	29.19	16.65
Day 13	8.030	6.482
Day 15	21.01	5.953
Day 16	15.69	7.567
Day 19	11.22	6.221
Day 20	12.30	10.23
Day 28	25.86	23.48

The variability never exceeds 30 %. It decreases when not considering the first measurement. Those are promising results. The variability should decrease even more with the new bubbling cell design, wherein FOX does not stagnate. Although the variability differs depending on the experiment day, the periodic determination of blanks during the measurement period would enable accurate OP measurements. The cause for the observed day-to-day variability of blank values could not be explained yet.

In future uses of the OP^{FOX} measuring device, blanks would happen every four or five cycles. The mean of blanks occurring before and after a measurement would be subtracted from the measurement.

3.3 Range of environmentally relevant concentrations for O_3, NO_2 and NO

The maximum levels of pollutants in the NABEL stations for all Switzerland from 2018 to 2021 are 121 $\mu g \cdot m^{-3}$ (120 ppb) for O_3, 361 $\mu g \cdot m^{-3}$ (189 ppb) for NO_2, and 521 $\mu g \cdot m^{-3}$ (418 ppb) for NO. These values allow choosing the range of assessed concentration for the O_3, NO_2, and NO experiments.

3.4 H_2O_2 liquid calibration

Two liquid H_2O_2 calibration curve were done, with the most complete given in fig. 3.7 (linear scale, corresponding to the second measurement serie). The linear regression obtained in the first experiment (0 $pmol$, 10 $pmol$, 100 $pmol$, 1000 $pmol$ is given in the appendix for information purposes (fig. .1). Note that for the first experiment, the first measurement of the standard solution at 0 $pmol$ was not considered as it was clearly an outlier. There might have been a problem with the OP measuring device for this measurement.
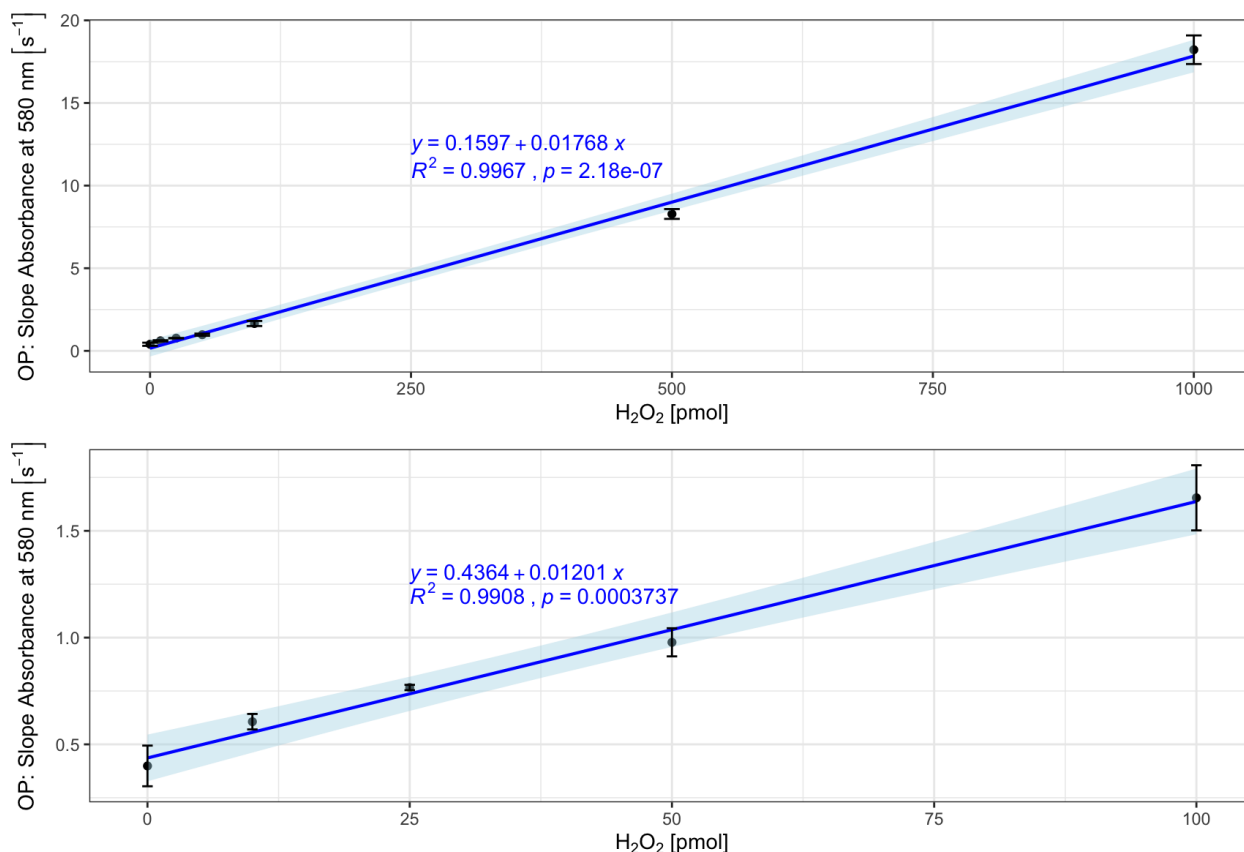
Figure 3.7: Liquid H_2O_2 calibration curve (in dark blue). The graph above is for the whole H_2O_2 range (0-1000 $pmol$). The graph below is for the range 0-100 $pmol$ H_2O_2. The points correspond to the mean of 5 repetitions, (except for the standard solution at 0 $pmol$, for which n=4) The repetitions standard deviations are displayed as error bars. The light blue shade around the curve corresponds to the 95 % confidence interval (CI)

A curve for the whole range (0-1000 $pmol$ H_2O_2) was established. As the ambient air OP values (see sections 3.9 and 3.10) corresponded to low H_2O_2 doses, a calibration for H_2O_2 range from 0 $pmol$ to 100 $pmol$ was established. Its regression equation ($OP: \; slope \; of \; absorbance \; at \; 580 \; nm \; = \; 0.01201 \cdot H_2O_2 \; [pmol] + 0.4364$) is used to convert the measured OP (slope of the absorbance at 580 nm) to H_2O_2 equivalents ($pmol$) for the subsequent results.

This calibration curve is also given with a log scale on the x-axis to allow for a good visualization (fig. 3.8). It should be noted that the 0 $pmol$ H_2O_2 dose has been shifted to 1 because 0 cannot be represented on a logarithmic scale due to the properties of the logarithmic function ($log(0)$ is not defined.) The graph with x-axis log scale for the first experiment is also given in the appendix (fig. .2).
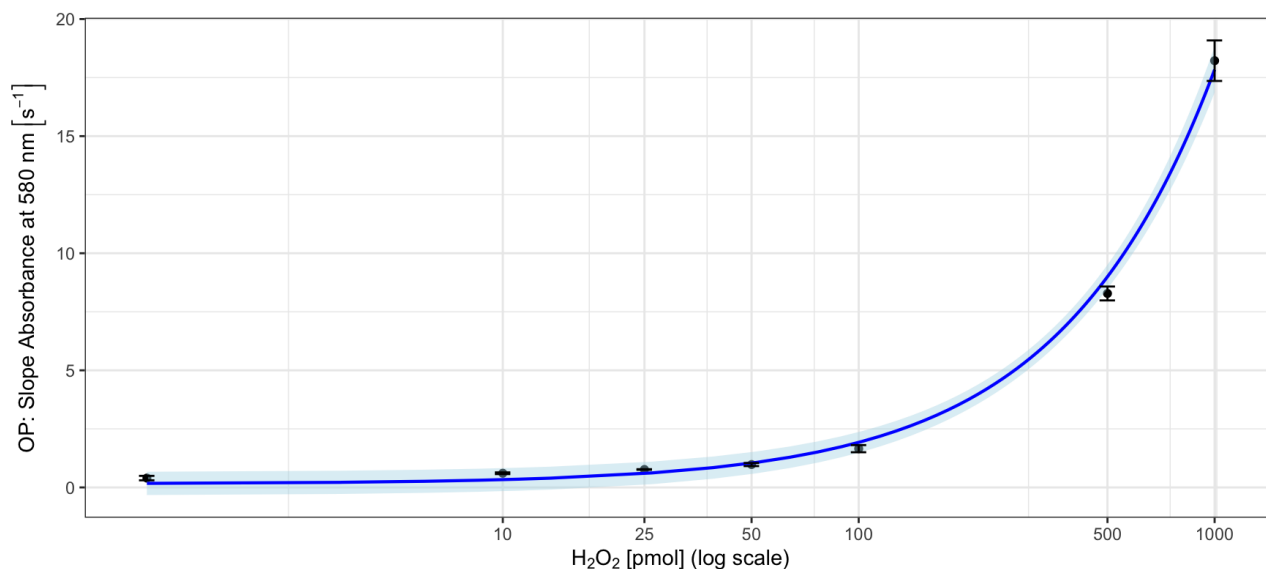
Figure 3.8: Liquid H_2O_2 calibration Curve (in dark blue) for the whole H_2O_2 range (0-1000 $pmol$). The x-axis scale is logarithmic. The points correspond to the mean of 5 repetitions, (except for the standard solution at 0 $pmol$, for which n=4) The repetitions standard deviations are displayed as error bars. The light blue shade around the curve corresponds to the 95 % confidence interval (CI)

It should be noted that, although the uncertainty on the measured OP is displayed as error bars, the computation of the regression line and associated 95 % CI does not consider these uncertainties.

The LOD and LOQ computed using the for the 0 pmol - 100 pmol H_2O_2 calibration curve are $LOD = 23.8$ $pmol$ H_2O_2 eq and $LOQ = 79.33$ $pmol$ H_2O_2 eq.

These findings are in line with the semi-quantitative LOD presented by Clark et al. [30], comprised between 10-50 $pmol$ H_2O_2 equivalent. These authors also used an aqueous standard solution of H_2O_2 for their calibration.

3.5 H_2O_2 gaseous calibration

The result of the H_2O_2 gaseous calibration is given in fig. 3.9.
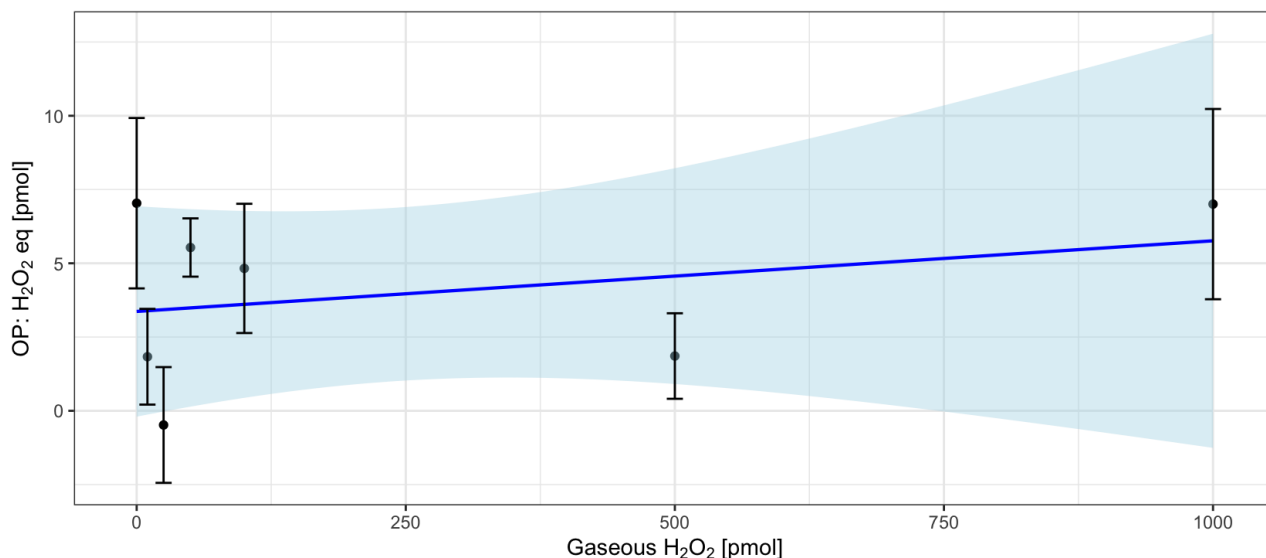
Figure 3.9: Gaseous H_2O_2 calibration curve (in dark blue). The points correspond to the mean of 5 repetitions. The measurement standard deviations are displayed as error bars. The light blue shade around the curve corresponds to the 95 % confidence interval (CI).

The calibration did not work well, as shown in fig. 3.9. Theoretically, gaseous H_2O_2 is expected to react similarly than liquid H_2O_2 (see fig. 3.7 and 3.8). This hypothesis should be verified with further experiments. One reason explaining the large observed variability in fig.3.9 is attributed to the generation of "gaseous" H_2O_2. Only 10 μL of an H_2O_2 standard solution were introduced in an atomizer (see Material and Methods, section 2.6) to produce an H_2O_2 suspension, which was aspirated in the bubbling cell. This volume is too low to allow a stable flux in the FOX and can also react with the surface of the tubing connecting the atomizer to the bubbling cell. Another factor that probably increased the measurement variability is that ambient air (with a variable oxidative potential) was pumped into the FOX solution alongside the gaseous H_2O_2. Due to lack of time, we could not improve this generation system, but we propose to increase the volume of the H_2O_2 standard solution in the atomizer.

3.6 O_3 calibration

The simultaneous evolution of OP^{FOX} and ozone concentration in the cabin during the first experiment are shown in fig. 3.10.
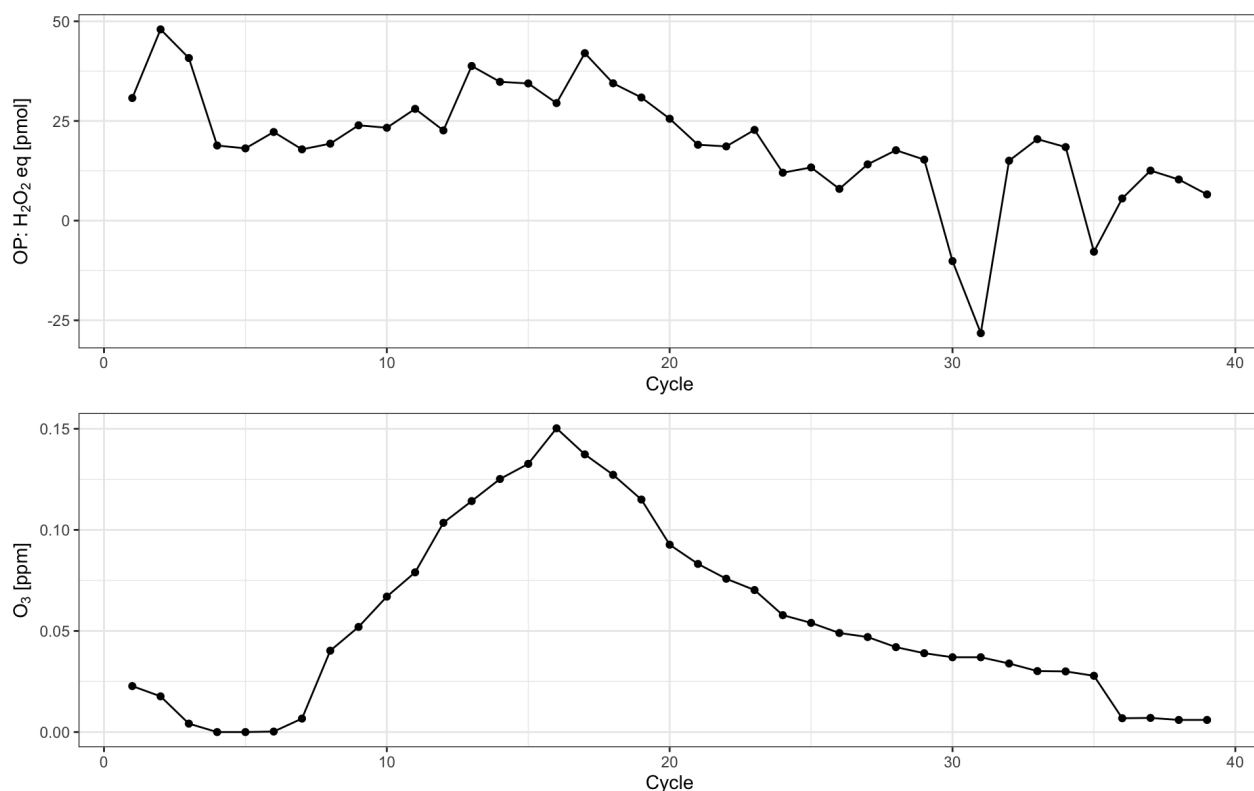
Figure 3.10: Simultaneous evolution of OP^{FOX} (higher panel) and O_3 concentration (lower panel) in the cabin

The OP seems to follow the same trend as the ozone concentration, although to a lesser extent, except for the low concentration at the beginning and the end of the experiment, where the OP was more variable. This variability might reflect the air variability brought by ventilation. The O_3 generation happens fast and does not allow taking many OP measurements. Note that the *Blank Bubbles* cycles are not shown here.

Three different calibration curves were established for O_3. One of them is presented in fig. 3.11 as illustrative purposes. The other ones can be found in the appendix (fig. .3 and .4). It should be noted that error bars are not displayed. As there are no repetition of the same assessed dose, standard deviations could not be computed.
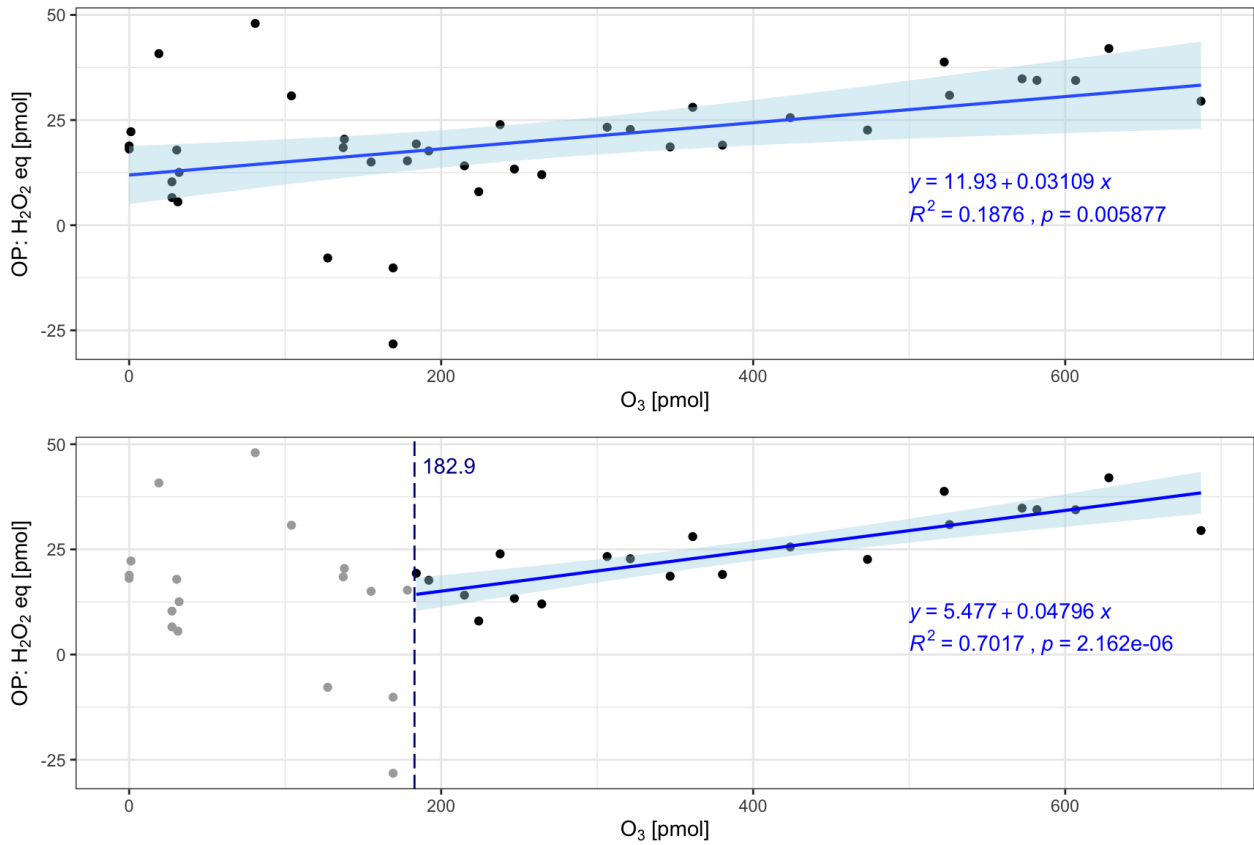
Figure 3.11: O_3 first calibration. The above panel regression considers every point. The regression below does not account for points (in grey) below a certain threshold (182.9 pmol O_3). The regression lines are displayed in blue. The light blue shading corresponds to the 95 % CI.

For O_3 levels below 180 *pmol*, some OP values expressed as H_2O_2 equivalent are observed to be negative. The ordinate at the origin of the calibration curve of liquid H_2O_2 (corresponding to the addition of D_2O in the bubbling cell) does not corresponds to what would be the O_3 zero (bubbling of ambient air from the cabin). Methodologically, the ideal calibration curve would have consisted of gaseous H_2O_2 diluted in ambient air from the cabin.

In Figure 3.11, a calibration is presented including all O_3 measurements (upper graph) whereas in the second calibration, only points above 182.9 *pmol* (corresponding to 40 *ppb* in the cabin) are used for the regression. This threshold was chosen because the ventilation of the cabin was switched on when O_3 levels reached this level of about 40 *ppb*. All the measurement points above this threshold were done without ventilation in the cabin. The regressions improve when considering O_3 doses above the 182.9 pmol limit. Therefore, those equations are used to compute O_3 sensitivity to the FOX assay relatively to liquid H_2O_2, the LOD, and LOQ. The results are displayed in table **??**.

Table 3: Regression equation, LOD, and LOQ for each of the calibration experiments

	regression equation	LOD [pmol O_3]	LOQ [pmol O_3]
1st calibration	OP = 0.04796·O_3 + 5.477	190.9	636.4
2nd calibration	OP = 0.0609·O_3 - 17.55	206.7	689.1
3rd calibration	OP = 0.04982·O_3 - 15.63	302.2	1007

The calibration curve slope average equals 0.05289. It can be interpreted as follows. The FOX

assay sensitivity to ozone is about 5 % of its sensitivity to liquid H_2O_2. The computed LOD and LOQ vary up to about a factor of 3.3 for LOD and 2 for LOQ depending on the regression equation used. The computed LOD and LOQ are likely very conservative. In fact, the intercept error is likely high because the calibration was extrapolated below 182.9 pmol.

The reason why the points below the 182.9 pmol O_3 follow the regression line poorly is not known with certainty. I hypothesize that other compounds than ozone were present when O_3 concentration was low. It is also probably the case during the whole experiments, but even more at the beginning and end of the experiments when the ventilation was on and brought ambient air in the cabin (see fig. 3.10). Moreover, the fact that the regressions are worse when considering low ozone concentration and other compounds supports the fact that O_3 does not play a leading role in the OP. The conditions when the ventilation was on simulated environmental conditions with low ozone concentration, other atmospheric pollutants, and wind, although the PM concentration might have varied less in the cabin than it may have in the environment.

The experiment protocol used here presents major drawback, consisting of a risk of cross-contamination. When establishing a calibration curve, low concentrations/doses are supposed to be assessed first. Here the O_3 concentration was first increased to about 150 ppb and then decreased. Not enough measurements could be taken during O_3 generation due to the speed of the process (see fig. 3.10), despite using the lowest possible electrical tension on the ozone generator. Higher ozone generator tension and ventilation combination were tested, hoping to increase ozone concentration more slowly. Unfortunately, ozone concentration could not be increased when the ventilation was on. The ideal experiment would have been to dilute a known ozone concentration in Tedlar bags with N_2. Unfortunately, O_3 was not available in a gas cylinder like NO_2 and NO. It had to be generated. Measuring the ozone concentration would have implied putting the ozone concentration measuring device *aeroqual* in a close recipient, which was hard to do. Moreover, ozone is unstable [45].

These findings confirm the results obtained by Clark et al. [30], who also observed (qualitatively) changes of OP^{FOX} in presence of O_3. In the present work, the sensitivity of the FOX assay to O_3 could be quantified and was observed to be about 20 times lower than for H_2O_2.

3.7   NO$_2$ calibration

The calibration results are presented in fig. 3.12.
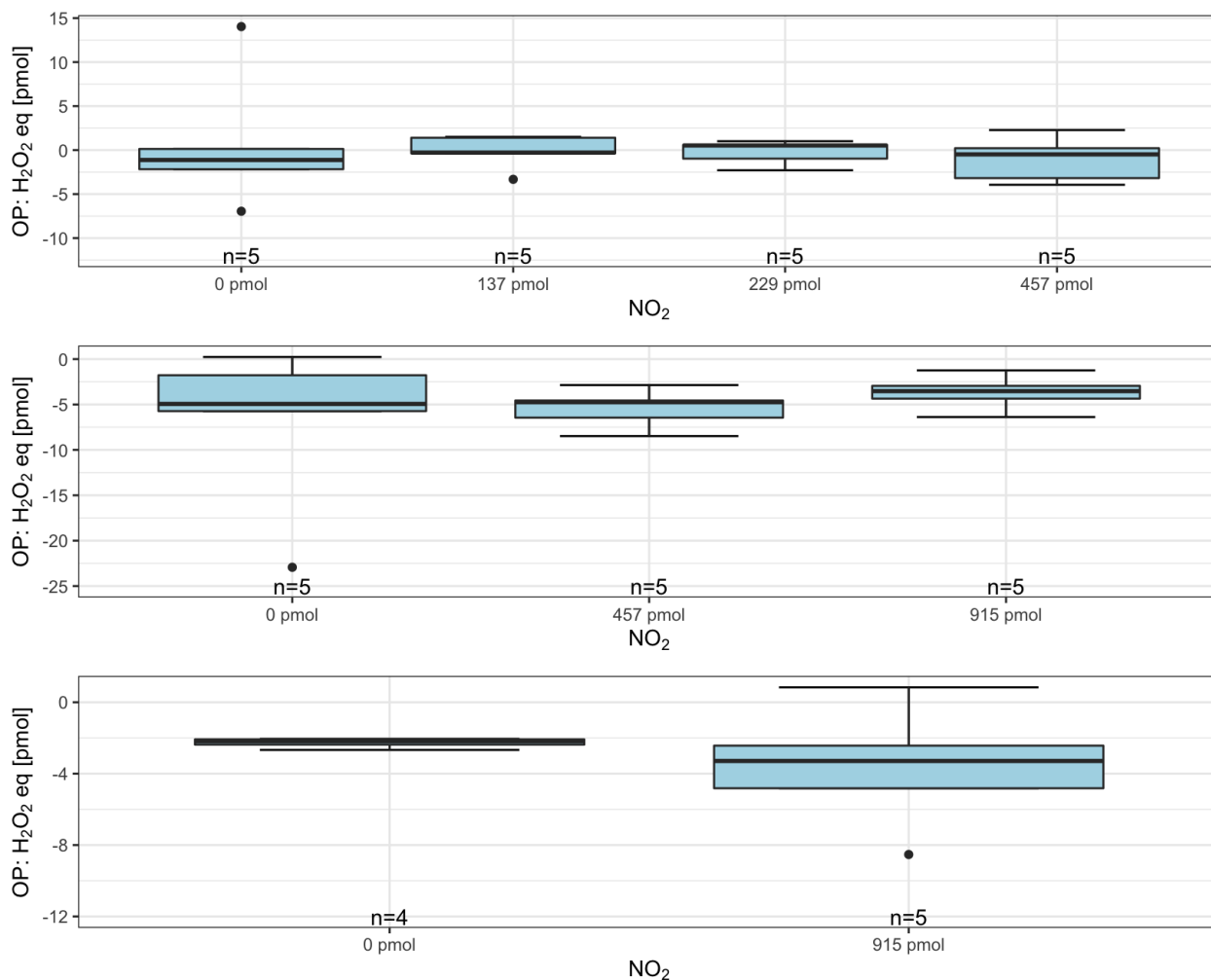
Figure 3.12: OP^{FOX} results for NO_2. First experiment (above panel), second experiment (middle panel), and third experiment (lower panel)

The assessed doses in the first experiment are low because they correspond to a range of daily maxima for some cantonal weather stations in Vaud. After this experiment, using hourly maxima for all NABEL stations from 2018 to 2021 was deemed more appropriate to determine the relevant range of pollutant concentrations.

The OP values expressed as H_2O_2 equivalent are sometimes negative. It is due to the use of the liquid H_2O_2 calibration curve to transform the absorbance slope at 580 nm in H_2O_2 eq. This calibration curve zero (D_2O) does not correspond to the NO_2 zero (technical laboratory air). Methodologically, the ideal calibration curve would have consisted of gaseous H_2O_2 diluted in laboratory air.

The assessed NO_2 doses do not seem to differ from the blank. This hypothesis is tested with the Mann-Whitney U test and is presented in Table 4.

Table 4: p-values and test interpretation for each NO_2 dose relative to the Blank (0 pmol)

Pair analyzed	p-value	Reject H_0 at $\alpha = 0.05$
0 *pmol* - 137 *pmol* First Experiment	0.69	No
0 *pmol* - 229 *pmol* First Experiment	0.55	No
0 *pmol* - 457 *pmol* First Experiment	1	No
0 *pmol* - 457 *pmol* Second Experiment	0.84	No
0 *pmol* - 915 *pmol* Second Experiment	0.84	No
0 *pmol* - 915 *pmol* Third Experiment	0.29	No

No assessed NO_2 dose is statistically significantly different from the respective experiment blank (0 *pmol*).

No calibration curve was established because the assessed NO_2 doses' OP responses are not unequivocally distinguishable (see fig. 3.12 and table 4).

NO_2 does not contribute to the OP^{FOX} signal. However, it does not mean that it does not affect health. It can cause respiratory system irritation and asthma [46]. Other OP assays could detect NO_2. To my knowledge, it has never been assessed, because of OP's focus on particles [7, 8, 21, 22].

3.8   NO calibration

The calibration results are presented in fig. 3.13.
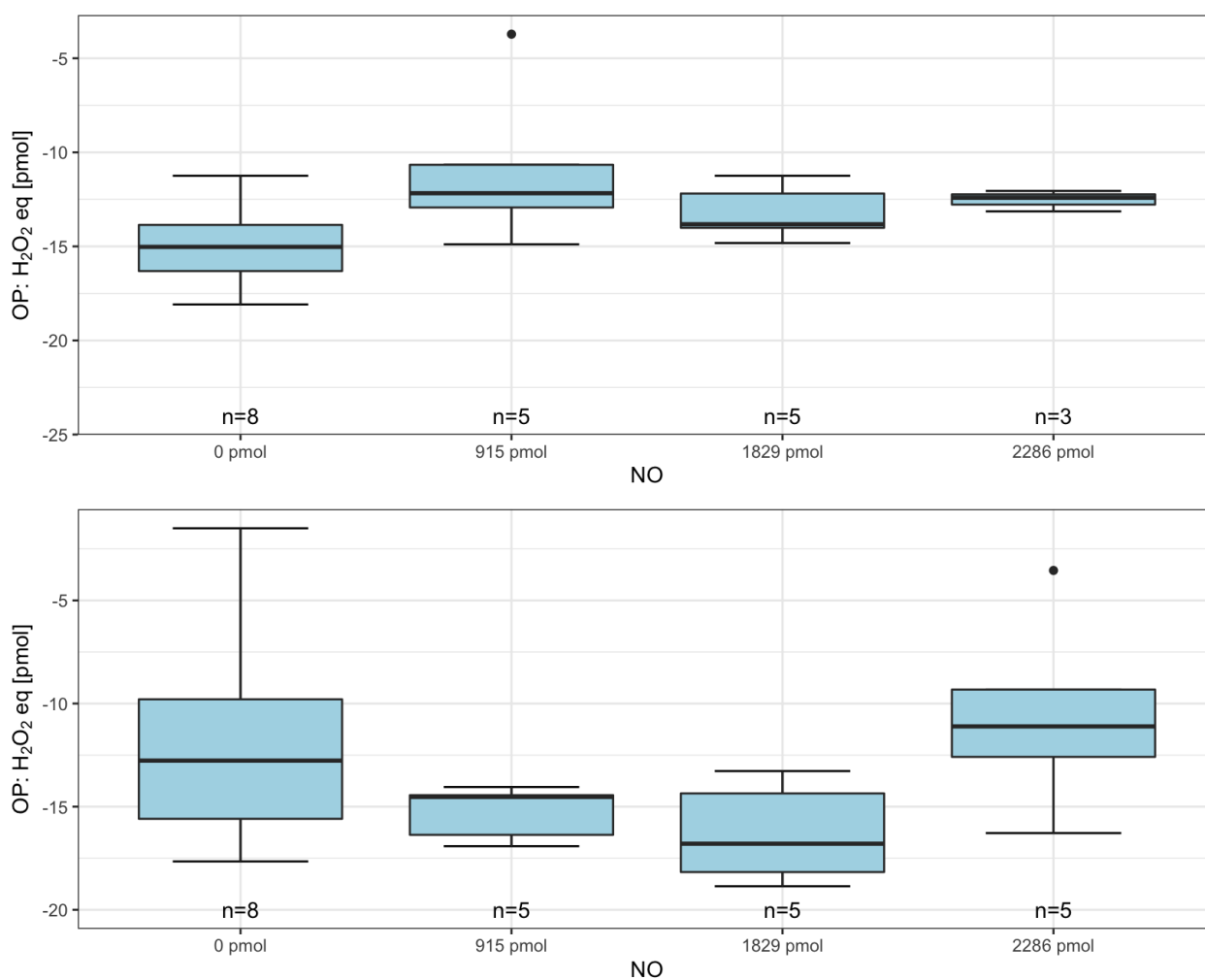
Figure 3.13: OP$^{\text{FOX}}$ results for NO. First experiment (above panel) and second experiment (lower panel)

The OP values expressed as H_2O_2 equivalent are sometimes negative. It is due to the use of the liquid H_2O_2 calibration curve to transform the absorbance slope at 580 nm in H_2O_2 eq. This calibration curve zero (D_2O) does not correspond to the NO zero (N_2). Methodologically, the ideal calibration curve would have consisted of gaseous H_2O_2 diluted in N_2.

The Mann-Whitney U test results are presented in the table **??**.

Table 5: p-values and test interpretation for each NO dose relative to the Blank (0 pmol)

Pair analyzed	p-value	Reject H_0 at $\alpha = 0.05$?
0 *pmol* - 915 *pmol* First Experiment	0.045	Yes
0 *pmol* - 1829 *pmol* First Experiment	0.19	No
0 *pmol* - 2286 *pmol* First Experiment	0.085	No
0 *pmol* - 915 *pmol* Second Experiment	0.22	No
0 *pmol* - 1829 *pmol* Second Experiment	0.093	No
0 *pmol* - 2286 *pmol* Second Experiment	0.72	No

Apart from the first experiment's 915 pmol NO, no assessed dose is statistically significantly different from the respective experiment blank (0 *pmol*).

No calibration curve was established because the assessed NO doses' OP responses are not unequivocally distinguishable (see fig. 3.13 and table ??).

NO does not contribute to the OP^{FOX} signal. However, it does not mean that it does not affect health. NO can turn to NO_2 when in contact with oxygen. Other OP assays could detect NO. To my knowledge, it has never been assessed, because of OP's focus on particles [7, 8, 21, 22].

3.9 Testing the OP measuring device prototype in ambient air conditions

The results for the ambient air OP measurement are presented in fig. 3.14.
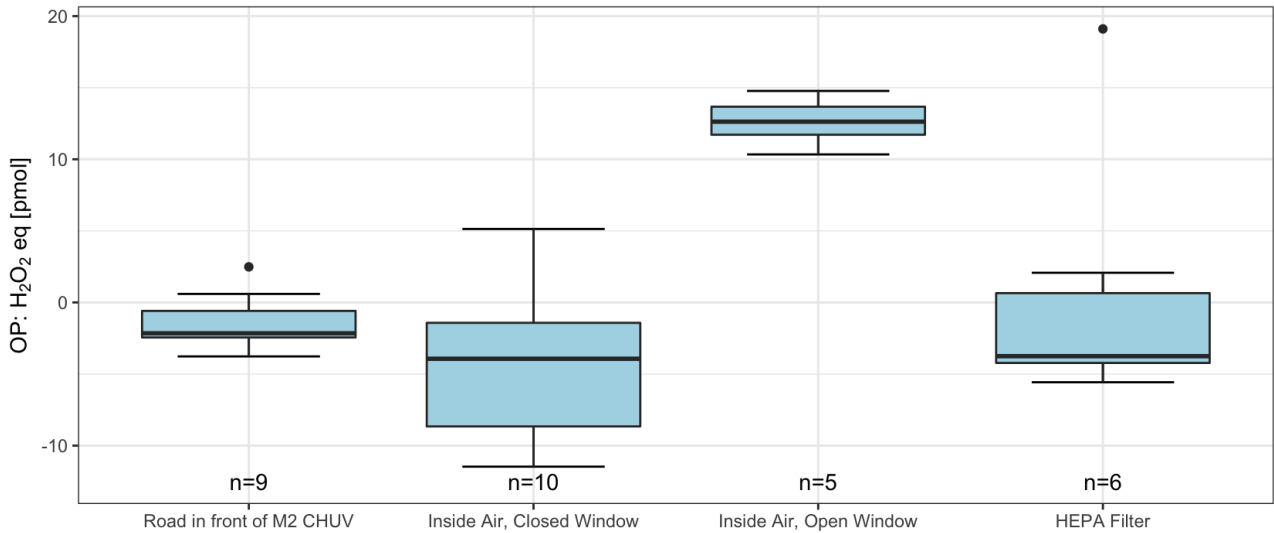
Figure 3.14: OP^{FOX} of ambient air measured in different configurations.

The Mann-Whitney U test results are presented in table 6

Table 6: p-values and test interpretation for ambient air measures

Pair analyzed	p-value	Reject H_0 at $\alpha = 0.05$
Road in front of M2 CHUV - Inside Air, Closed Window	0.11	No
Road in front of M2 CHUV - Inside Air, Open Window	0.00010	Yes
Road in front of M2 CHUV - HEPA Filter	0.33	No
Inside Air, Closed Window - Inside Air, Open Window	0.00067	Yes
Inside Air, Closed Window - HEPA Filter	0.43	No
Inside Air, Open Window - HEPA Filter	0.082	No
Inside Air, Open Window - HEPA Filter without the first measurement	0.0079	Yes

The use of HEPA filter made the OP value to decrease at a level close to the one observed for closed windows. This fact supports the assumption that the OP was predominantly due to PM in this case. The HEPA filter outsider point corresponds to the first measurement (see fig. 3.14). It is probably high because of previous measurements' influence. Another explanation (although less likely) would be that the filter was slightly dirty. It is worth noting that the open window and HEPA filter measurements are not significantly different when considering all data (see Table 6). Removing the first measurement (clearly, an outlier, see fig. 3.14) leads to the observation that the inside air with the window opened corresponds to a statistically significant increase of OP^{FOX}.

This experiment shows that the OP^{FOX} measuring device prototype can detect air quality changes in the environment, such as the presence of a nearby construction work.

It must be noted that some OP values expressed in H_2O_2 equivalent are negative. It is due to the use of the liquid H_2O_2 calibration curve to transform the absorbance slope at 580 nm in H_2O_2 eq. This calibration curve zero (D_2O) does not correspond to the experiment zero (ambient air). Methodologically, the ideal calibration curve would have consisted of gaseous H_2O_2 diluted in ambient air.

3.10 Testing the OP measuring device prototype in an occupational health context

The results for the on-line measurements at the watchmaking factory are presented as boxplots in fig. 3.15.
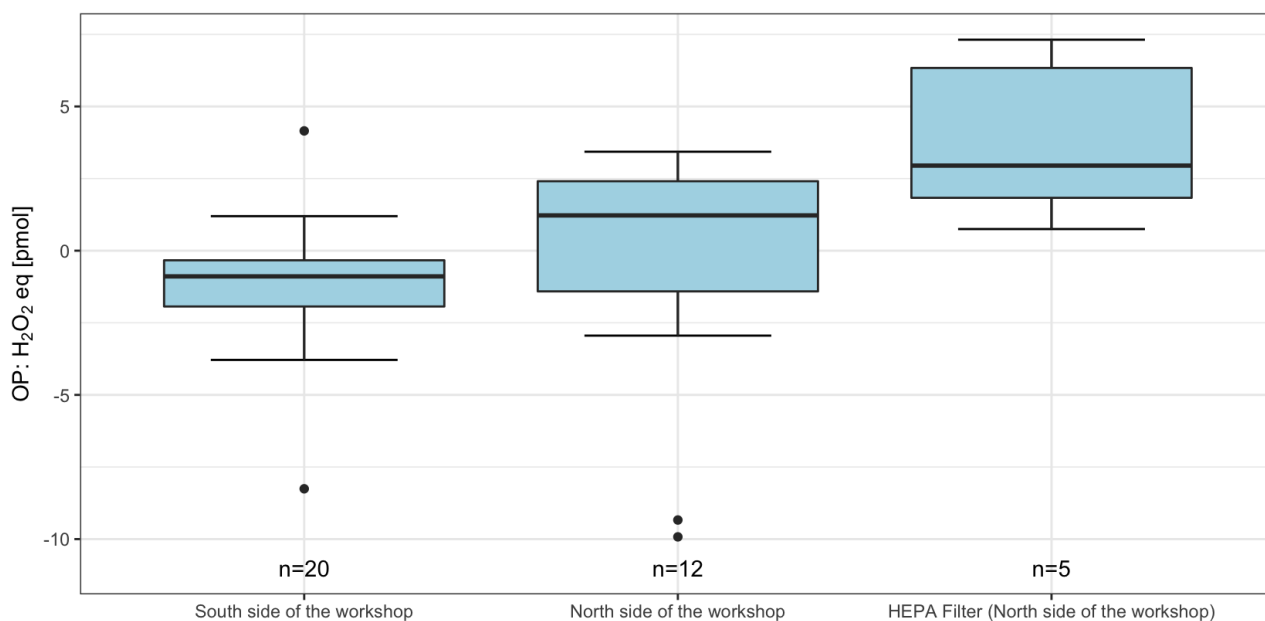
Figure 3.15: OP^{FOX} for the on-line measurements at the watchmaking factory

The OP values expressed as H_2O_2 equivalent are sometimes negative. It is due to the use of the liquid H_2O_2 calibration curve to transform the absorbance slope at 580 nm in H_2O_2 eq. This calibration curve zero (D_2O) does not correspond to the workshop zero (ambient air). Methodologically, the ideal calibration curve would have consisted of gaseous H_2O_2 diluted in ambient air from the workshop.

The north side measurements seem a little higher than the south side ones but are not statistically significantly different (see Table **??**). The measurements with the HEPA filter (north side) is similar to the OP measured at the north side but significantly higher than the south site (see Table **??**).

Table 7: p-values and test interpretation for the on-line measurement at the watchmaking factory

Pair analyzed	p-value	Reject H_0 at $\alpha = 0.05$
South Side - North Side	0.11	No
North Side - HEPA Filter	0.091	No
South Side - HEPA Filter	0.00045	Yes

Although the difference between the north side measurements with and without the HEPA filter is not statistically significantly different, it can be seen graphically that the measurements with the HEPA filter are slightly higher. One would have expected a lower OP once the particles are removed. Assuming the filter was clean and working well, an explanation would be that the gaseous OP fraction alone was higher than the total (gaseous + particulate) OP. The particles might have inhibited the gaseous OP contribution. Indeed, a sampling of the total aerosol at both north and south sites through a desorption tube and its subsequent analysis using the thermodesorption GC-MS technique indicated the presence of butylated hydroxytoluene. This compound is known to act as an antioxidant and could be present as an additive in the metalworking fluid used in this atelier. Its presence in the particulate phase could interfere with the FOX assay, by hindering the Fe^{2+} to Fe^{3+} oxidation. However, those are only assumptions at this stage. Other measurements should be taken to verify if the OP increased with a filter (only five repetitions were taken with the HEPA filter). It might be random (remember that the difference was not statistically significantly different).

In parallel to these on-line measurements, sampling with filters at the same sites was achieved to compare off-line with on-line results. The OP off-line measurement results are presented in table 8.

	Intrinsic OP [$pmol\ H_2O_2\ eq\ \cdot \mu g^{-1}$]	Volumetric OP [$pmol\ H_2O_2\ eq \cdot m^{-3}$]
South side of the workshop	32.4	16418.5
North side of the workshop	< LOD	< LOD

Table 8: Results for the off-line measurements at the watchmaking factory

The off-line measurements detected OP on the south side of the workshop but not on the north side. These results contradict the on-line measurements, where the south and north side measurements did not significantly differ.

Further measurement campaigns should be deployed in a similar industry to strenghten the observed results.

It should be noted that on-line OP values were expressed as H_2O_2 equivalent (like the other results shown in this report). However, to better compare them with the off-line measurements, they could be expressed in H_2O_2 equivalent per volume unit using the volume sampled during the bubbling phase. Furthermore, the on-line OP measuring device could be equipped with a direct-reading instrument for PM, allowing the expression of the OP as H_2O_2 equivalent per PM mass unit.

3.11   Perspectives

During this master thesis, development and characterization of the online OP measuring device were partly achieved. The current prototype is improved and already enables automated determination of ambient OP over several hours. In future work, several points should be addressed to improve the accuracy of the OP measurements and understand in depth the environmental variables which contribute to it:

1) Establish a calibration with gaseous H_2O_2 based on an improved experimental setup (larger volume of liquid H_2O_2 in an atomizer)

2) Stronger self-reference measurement data are expected using a near-IR LED at 950 nm with no overlap with the absorbance domain of the FOX assay

3) Evaluate the prototype reactivity to a series of lab-generated particles and simulate the aging effect (UV, O_3, etc.)

4) Perform measurement campaigns at an air quality station (Plaines-du-Loup, Lausanne) to correlate ambient OP with air pollutants (PM_{10}, $PM_{2.5}$, O_3, NO_2, NO_x, etc.) and meteorological conditions (temperature, pressure, wind) at different seasons and time.

Finally, the correlation between the FOX assay reactivity and health issues should be investigated. Is the ambient air OP measured by the FOX assay a good predictor of cardiovascular and respiratory health? If yes, it would confirm its usefulness as an air pollution metric. Some studies have investigated the OP^{FOX} of exhaled air [26, 28]. There is a body of literature regarding other OP assays' (e.g., AA, DTT) use in epidemiological studies [7, 8]. But to my knowledge, so far, no epidemiological studies regarding ambient air OP^{FOX} have been realized. The OP^{FOX} could be measured at different places and related to epidemiological information about cardiovascular and respiratory health. Geographic Information Systems (GIS) would help carry out those tasks.

4   Conclusion

During this master thesis, a prototype measuring ambient air OP was improved and used to assess the response of the FOX assay toward different gases and ambient air conditions.

The main improvements consisted of a LED-based level detector to control the FOX level in the bubbling cell, a filter and a valve to protect the air pump from FOX and control the bubbling air flow, the transition from a horizontal to a vertical measurement cell, and various improvements on the CoolTerm Interface allowing a better instrument control and data management. Other improvements, such as the design of a new bubbling cell avoiding FOX stagnation and the addition of a valve allowing switching to different air inlets, were newly added and are still being tested.

The use of a *blank bubble* (i.e., no air impinged into the FOX) was discussed as blank to be subtracted from the measurement. Liquid H_2O_2 was used to established a calibration curve. A calibration with gaseous H_2O_2 was attempted, but the experiment protocol needs refining. The FOX assay sensitivity to O_3 was determined to be about 5 % relatively to liquid H_2O_2. In turn, NO_x (NO_2 and NO) did not react to the FOX assay and will not contribute to the OP measurements. Interestingly, the OP measuring device prototype could detect changes in air quality, such as the presence of a nearby construction site.

The on-line OP^{FOX} measuring method (gas+PM) used here did not match the results of an off-line method (PM) during a measurement campaign at a watchmaking factory, showing that particulate and gas components of complex aerosols can exhibit singular OP behavior. Further experiments are needed to explore the contribution of all aerosol components in specific situations.

Significant improvements on the prototype and a deepened understanding of the FOX reactivity to different gases and ambient air conditions have been achieved during this work, but still further explorations remains to fully characterize the online OP prototype. The prototype will be further developed in terms of instrumentation (e.g. dual air sampling, bubbling cell downsizing, internal led reference). For instance the calibration of the current prototype with gaseous H_2O_2 is still challenging but will enable a correct conversion of raw data into H_2O_2 equivalents unit. The OP^{FOX} reactivity to different kinds of PM and mixtures of gases and PM under different environmental conditions should be assessed, both in the laboratory and during a measurement campaign at a air quality station. Finally, the relevance of the OP^{FOX} assay as an air pollution metric relative to health shall be investigated in future epidemiological studies.

5 Acknowledgments

The achievement of this master thesis would not have been possible without the help of many people I want to thank hereafter.

Dr. Guillaume Suarez and Dr. Jean-Jacques Sauvain, who accompanied me throughout this project, supervised it and reviewed my report before the deadline. They taught me a lot, gave me good advice and gave me a lot of freedom and responsibility to carry out this project. Thanks for your help and your trust. Thank you for teaching me that struggling to design experiments and to make sense of your results is part of the process of scientific research.

Dr. Florian Breider who agreed to be my EPFL supervisor and who taught me a lot about lab work during a semester project last semester.

Dr. Nicolas Concha-Lozano, from *Centre Universitaire Romand de Médecine Légale (CURML)* who astutetly implemented the improvements on the OP^{FOX}.

Prof. David Vernez, who sparked my interest who environmental and occupational health thanks to it EPFL class *Santé environnementale, santé au travail* and gave me the opportunity to carry out my master thesis at *Unisanté, Département santé, travail et Environnement.*

Antonio Toto, my collegue at Unisanté who designed the new bubbling cell and piece that holds it.

My collegue Dr. Maud Hemmendinger for your help in the lab and with the programming language R.

Vivane Remy, my collegue at Unisanté and study friend for your advice and resources on the project.

My other collegues at Unisanté and from CURML who were always ready to help: Hélène (thank for offering your help with the graphs realization and the oral exam preparation), Nicole (thank you for letting me borrow a lunch box during the last six months), Nicolas, Abrar, Bianca, Sylvain, Gregory Simon, Christine Renaud, Sophie, Sylvia Guilllaume.

Thank you to all the people mentioned above for the wonderful lunches, coffee breaks, interesting conversations and laughs.

Thank you to my EPFL friends Sarah Courdier and Alexandre Fourrier who answered my general questions about master theses.

Last but not least, a huge thanks to my family who supported my financially and emotionally during my bachelor and master studies: my mum Isabelle, my dad François, my sister Fanny,my brother Théo, my cat Shifu and my maternal grandparents, Georges and Mercedes, who let me crash at their place more time than I can count.
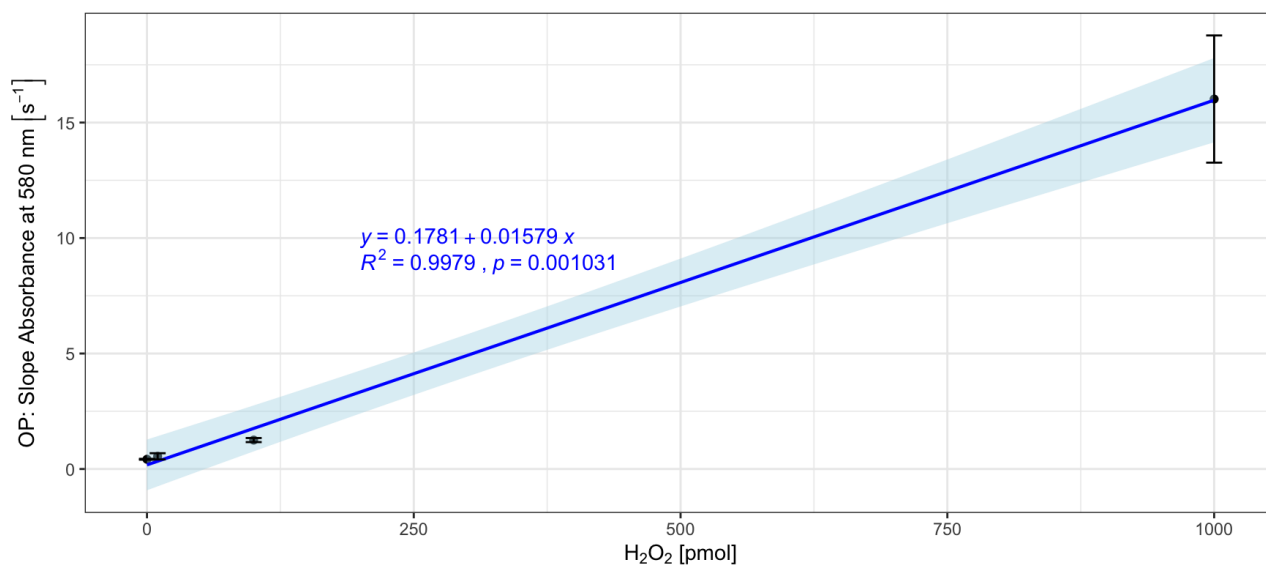
Appendices

Figure .1: First experiment liquid H_2O_2 calibration curve (in dark blue) for the whole H_2O_2 range (0-1000 $pmol$). The points correspond to the mean of each measurement. The measurement standard deviations are displayed as error bars. The light blue shade around the curve corresponds to the 95 % confidence interval (CI)

Figure .2: First experiment liquid H_2O_2 calibration curve (in dark blue) for the whole H_2O_2 range (0-1000 $pmol$). The x-axis scale is logarithmic. The points correspond to the mean of each measurement. The measurement standard deviations are displayed as error bars. The light blue shade around the curve corresponds to the 95 % confidence interval (CI)
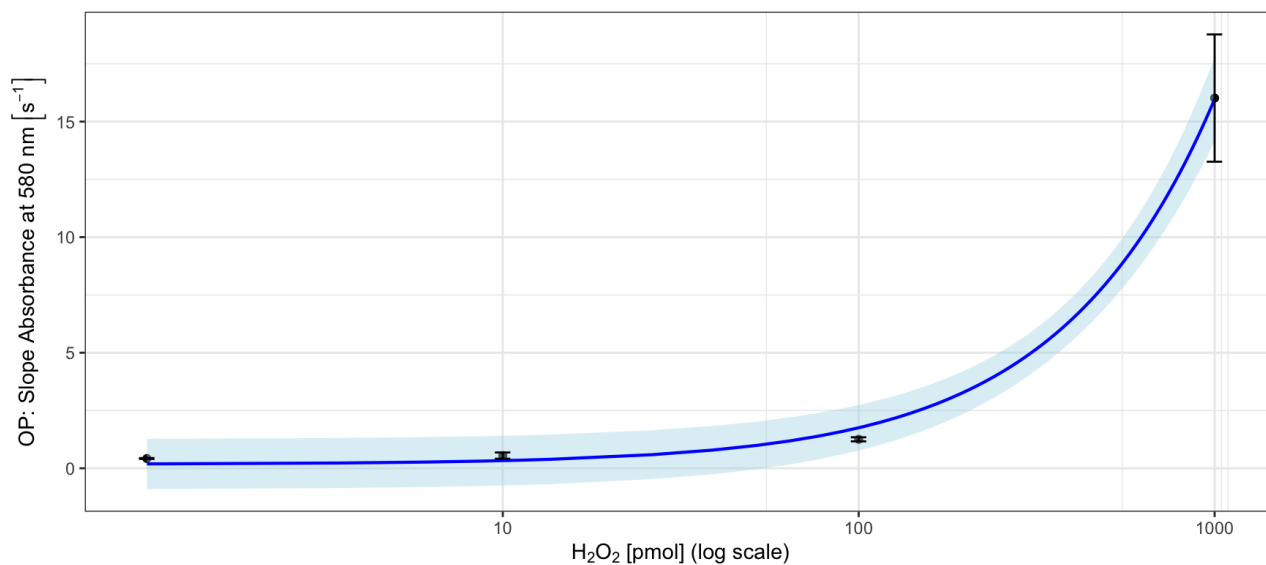
Figure .3: O_3 second calibration. The above panel regression considers every point. The regression below does not account for points (in grey) below a certain threshold (182.9 pmol). The regression lines are displayed in blue. The light blue shading corresponds to the 95 % CI.
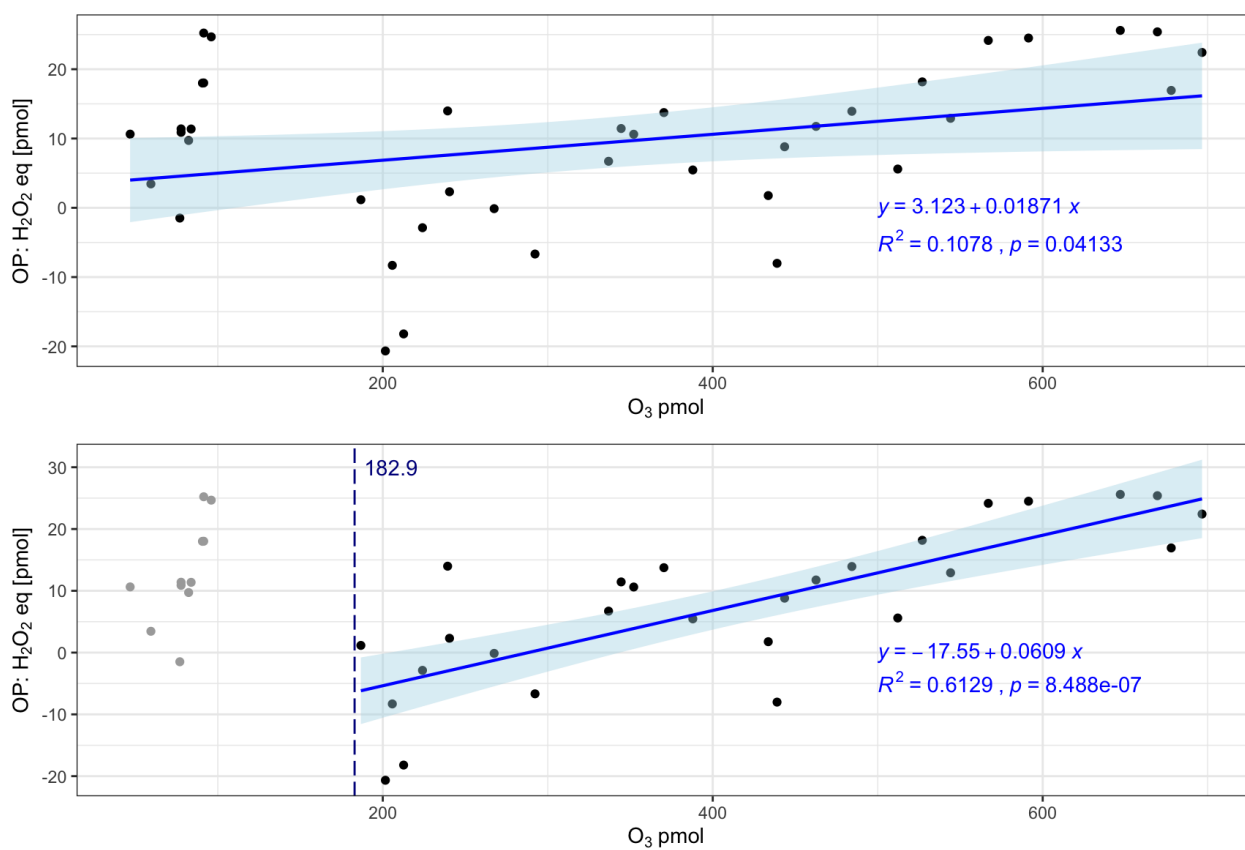
Figure .4: O_3 third calibration. The above panel regression considers every point. The regression below does not account for points (in grey) below a certain threshold (182.9 pmol). The regression lines are displayed in blue. The light blue shading corresponds to the 95 % CI.
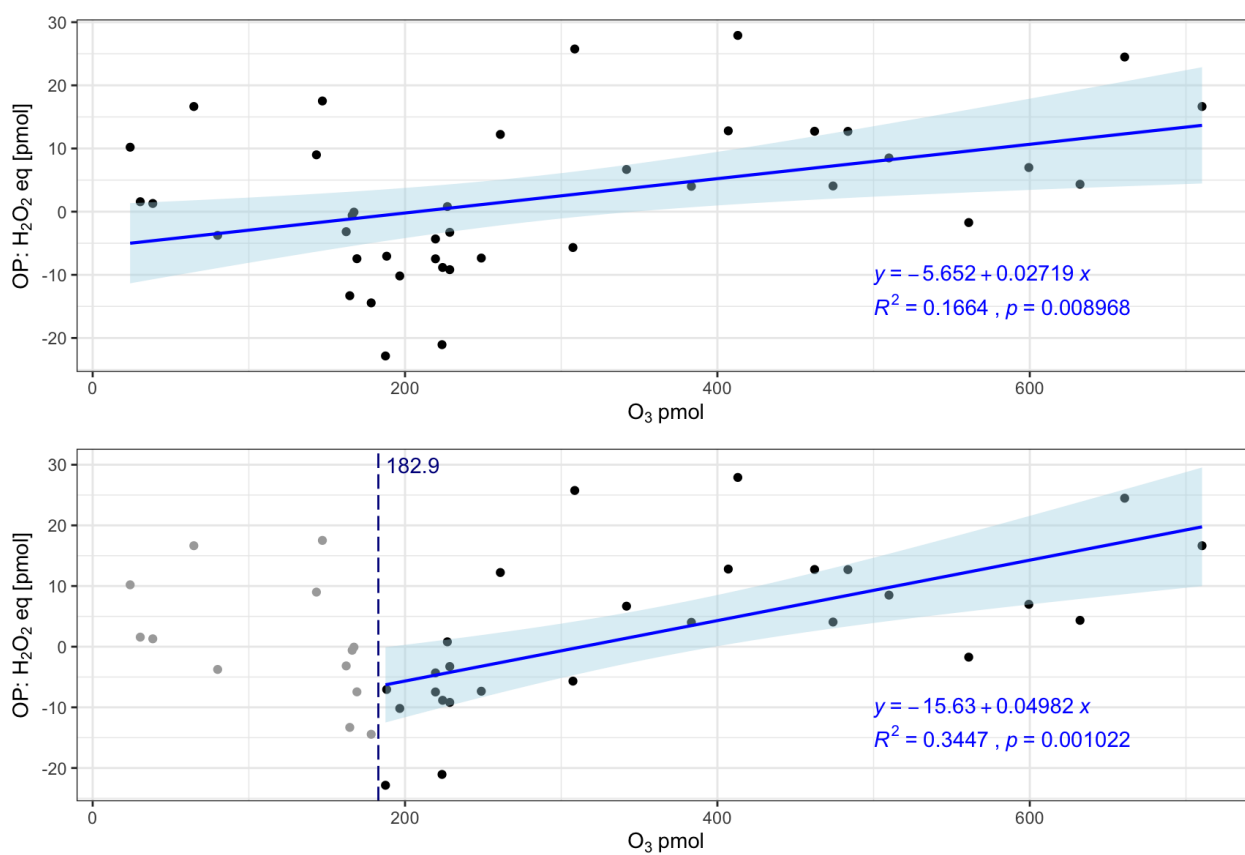
References

[1] World Health Organization (WHO), *Air pollution*, en. [Online]. Available: https://www.who.int/health-topics/air-pollution (visited on 05/10/2022).

[2] F. O. f. t. E. FOEN, *Effects of air pollution on health*, en. [Online]. Available: https://www.bafu.admin.ch/bafu/en/home/themen/thema-luft/luft--fachinformationen/auswirkungen-der-luftverschmutzung/auswirkungen-der-luftverschmutzung-auf-die-gesundheit.html (visited on 05/10/2022).

[3] O. f. d. l. OFEV, *Air: En bref*, fr. [Online]. Available: https://www.bafu.admin.ch/bafu/fr/home/themen/thema-luft/luft--das-wichtigste-in-kuerze.html (visited on 08/02/2022).

[4] O. US EPA, *Indoor Air Quality*, en, Reports and Assessments, Nov. 2017. [Online]. Available: https://www.epa.gov/report-environment/indoor-air-quality (visited on 08/02/2022).

[5] O. f. d. l. s. p. OFSP, *Polluants d'intérieur et problèmes de santé*, fr. [Online]. Available: https://www.bag.admin.ch/bag/fr/home/gesund-leben/umwelt-und-gesundheit/wohngifte/wohngifte-und-gesundheitliche-beschwerden.html (visited on 08/02/2022).

[6] O. f. d. l. OFEV, *Effets de la pollution atmosphérique sur la santé*, fr. [Online]. Available: https://www.bafu.admin.ch/bafu/fr/home/themen/thema-luft/luft--fachinformationen/auswirkungen-der-luftverschmutzung/auswirkungen-der-luftverschmutzung-auf-die-gesundheit.html (visited on 05/24/2022).

[7] D. Gao, S. Ripley, S. Weichenthal, and K. J. Godri Pollitt, "Ambient particulate matter oxidative potential: Chemical determinants, associated health effects, and strategies for risk management," en, *Free Radical Biology and Medicine*, vol. 151, pp. 7–25, May 2020, ISSN: 08915849. DOI: 10.1016/j.freeradbiomed.2020.04.028. [Online]. Available: https://linkinghub.elsevier.com/retrieve/pii/S0891584920308261 (visited on 03/04/2022).

[8] J. T. Bates *et al.*, "Review of Acellular Assays of Ambient Particulate Matter Oxidative Potential: Methods and Relationships with Composition, Sources, and Health Effects," en, *Environmental Science & Technology*, vol. 53, no. 8, pp. 4003–4019, Apr. 2019, ISSN: 0013-936X, 1520-5851. DOI: 10.1021/acs.est.8b03430. [Online]. Available: https://pubs.acs.org/doi/10.1021/acs.est.8b03430 (visited on 03/04/2022).

[9] World Health Organization (WHO), *Ambient (outdoor) air pollution*, en. [Online]. Available: https://www.who.int/news-room/fact-sheets/detail/ambient-(outdoor)-air-quality-and-health (visited on 08/02/2022).

[10] *SR 814.318.142.1 - Ordinance of 16 December 1985 on Air Pollution Control (OAPC)*. [Online]. Available: https://www.fedlex.admin.ch/eli/cc/1986/208_208_208/en.

[11] Asst. Prof. Dusan Licina, Ph.D., *Indoor air quality and ventilation - Introduction to the topic (EPFL course)*, Feb. 2022.

[12] *SR 814.501 - Radiological Protection Ordinance of 26 April 2017 (RPO)*. [Online]. Available: https://www.fedlex.admin.ch/eli/cc/2017/502/en (visited on 08/02/2022).

[13] *RS 818.31 - Loi fédérale du 3 octobre 2008 sur la protection contre le tabagisme passif*. [Online]. Available: https://www.fedlex.admin.ch/eli/cc/2009/766/fr (visited on 08/02/2022).

[14] Unisanté, *Interdiction de fumer dans les lieux publics, Législation — Tabagisme*, fr-FR. [Online]. Available: https://tabagisme.unisante.ch/category/legislation/interdiction-de-fumer-dans-les-lieux-publics/ (visited on 08/02/2022).

[15] O. f. d. l. OFEV, *Requête de données NABEL*, fr. [Online]. Available: https://www.bafu.admin.ch/bafu/fr/home/themen/thema-luft/luft--daten--indikatoren-und-karten/luftbelastung--daten/datenabfrage-nabel.html (visited on 08/06/2022).

[16] Marco Steiger *et al.*, *Cercl'Air Recommandation 27a Indice de pollution de l'air à court terme IPC*, fr, Dec. 2020.

[17] Markus Camenzind *et al.*, *Cercl'Air Recommandation N°27b Indice de pollution de l'air à long terme IPL*, Jun. 2015.

[18] O. US EPA, *Particulate Matter (PM) Basics*, en, Overviews and Factsheets, Apr. 2016. [Online]. Available: https://www.epa.gov/pm-pollution/particulate-matter-pm-basics (visited on 05/24/2022).

[19] J. G. Ayres *et al.*, "Evaluating the Toxicity of Airborne Particulate Matter and Nanoparticles by Measuring Oxidative Stress Potential—A Workshop Report and Consensus Statement," en, *Inhalation Toxicology*, vol. 20, no. 1, pp. 75–99, Jan. 2008, ISSN: 0895-8378, 1091-7691. DOI: 10.1080/08958370701665517. [Online]. Available: http://www.tandfonline.com/doi/full/10.1080/08958370701665517 (visited on 08/25/2022).

[20] C. C. f. O. H. a. S. Government of Canada, *How Do Particulates Enter the Respiratory System? : OSH Answers*, eng, Last Modified: 2018-01-03, Aug. 2022. [Online]. Available: https://www.ccohs.ca/oshanswers/chemicals/how_do.html (visited on 08/26/2022).

[21] S. Stevanovic *et al.*, "Oxidative potential of gas phase combustion emissions - An underestimated and potentially harmful component of air pollution from combustion processes," en, *Atmospheric Environment*, vol. 158, pp. 227–235, Jun. 2017, ISSN: 13522310. DOI: 10.1016/j.atmosenv.2017.03.041. [Online]. Available: https://linkinghub.elsevier.com/retrieve/pii/S1352231017302108 (visited on 08/03/2022).

[22] J.-J. Sauvain *et al.*, "Oxidative potential of aerosolized metalworking fluids in occupational settings," en, *International Journal of Hygiene and Environmental Health*, vol. 235, p. 113 775, Jun. 2021, ISSN: 14384639. DOI: 10.1016/j.ijheh.2021.113775. [Online]. Available: https://linkinghub.elsevier.com/retrieve/pii/S1438463921000900 (visited on 05/13/2022).

[23] C. Gay, J. Collins, and J. M. Gebicki, "Hydroperoxide Assay with the Ferric–Xylenol Orange Complex," en, *Analytical Biochemistry*, vol. 273, no. 2, pp. 149–155, Sep. 1999, ISSN: 00032697. DOI: 10.1006/abio.1999.4208. [Online]. Available: https://linkinghub.elsevier.com/retrieve/pii/S0003269799942082 (visited on 03/04/2022).

[24] C. Gay and J. M. Gebicki, "A Critical Evaluation of the Effect of Sorbitol on the Ferric–Xylenol Orange Hydroperoxide Assay," en, *Analytical Biochemistry*, vol. 284, no. 2, pp. 217–220, Sep. 2000, ISSN: 00032697. DOI: 10.1006/abio.2000.4696. [Online]. Available: https://linkinghub.elsevier.com/retrieve/pii/S0003269700946967 (visited on 03/04/2022).

[25] R. Bou, R. Codony, A. Tres, E. A. Decker, and F. Guardiola, "Determination of hydroperoxides in foods and biological samples by the ferrous oxidation–xylenol orange method: A review of the factors that influence the method's performance," en, *Analytical Biochemistry*, vol. 377, no. 1, pp. 1–15, Jun. 2008, ISSN: 00032697. DOI: 10.1016/j.ab.2008.02.029. [Online]. Available: https://linkinghub.elsevier.com/retrieve/pii/S0003269708001103 (visited on 05/13/2022).

[26] A. Laulagnet, J. Sauvain, N. Concha-Lozano, M. Riediker, and G. Suárez, "Sensitive Photonic System to Measure Oxidative Potential of Airborne Nanoparticles and ROS Levels in Exhaled Air," en, *Procedia Engineering*, vol. 120, pp. 632–636, 2015, ISSN: 18777058. DOI: 10.1016/j.proeng.2015.08.659. [Online]. Available: https://linkinghub.elsevier.com/retrieve/pii/S187770581502322X (visited on 03/04/2022).

[27] D. Vernez *et al.*, "Airborne nano-TiO 2 particles: An innate or environmentally-induced toxicity?" en, *Journal of Photochemistry and Photobiology A: Chemistry*, vol. 343, pp. 119–125, Jun. 2017, ISSN: 10106030. DOI: 10.1016/j.jphotochem.2017.04.022. [Online]. Available: https://linkinghub.elsevier.com/retrieve/pii/S1010603017302320 (visited on 03/04/2022).

[28] S. Goekce *et al.*, "Multiscattering-enhanced absorbance to enable the sensitive analysis of extremely diluted biological samples: Determination of oxidative potential in exhaled air," en, *Medicine in Novel Technology and Devices*, vol. 14, p. 100 120, Jun. 2022, ISSN: 25900935. DOI: 10.1016/j.medntd.2022.100120. [Online]. Available: https://linkinghub.elsevier.com/retrieve/pii/S2590093522000078 (visited on 05/12/2022).

[29] S. Caquot and V. Remy, "Design Project: Caractérisation d'un prototype permettant la mesure du potentiel oxydant de l'air ambiant (Rapport final)," Français, EPFL - Unisanté, Tech. Rep., 2020.

[30] J. Clark and A. Perriard, "Design Project: Caract erisation d'un prototype permettant la mesure du potentiel oxydant de l'air ambiant (Rapport final)," Français, EPFL - Unisanté, Tech. Rep., 2021.

[31] Dr. Sauvain Jean-Jacques and Dr. Suarez Guillaume, *Promotion des technologies environnementales Demande de subside: Testing of a direct reading instrument for oxidative potential measurement (DIROP)*.

[32] M. C. Pietrogrande, D. Bacco, A. Trentini, and M. Russo, "Effect of filter extraction solvents on the measurement of the oxidative potential of airborne PM2.5," en, *Environmental Science and Pollution Research*, vol. 28, no. 23, pp. 29 551–29 563, Jun. 2021, ISSN: 0944-1344, 1614-7499. DOI: 10.1007/s11356-021-12604-7. [Online]. Available: https://link.springer.com/10.1007/s11356-021-12604-7 (visited on 08/05/2022).

[33] J.-J. Sauvain, S. Deslarzes, F. Storti, and M. Riediker, "Oxidative Potential of Particles in Different Occupational Environments: A Pilot Study," en, *Annals of Occupational Hygiene*, vol. 59, no. 7, pp. 882–894, Aug. 2015, ISSN: 0003-4878, 1475-3162. DOI: 10.1093/annhyg/mev024. [Online]. Available: https://academic.oup.com/annweh/article-lookup/doi/10.1093/annhyg/mev024 (visited on 08/05/2022).

[34] Z. Jun *et al.*, "Development, characterization and first deployment of an improved online reactive oxygen species analyzer," en, 16 p. Jan. 2018, Artwork Size: 16 p. Medium: application/pdf Publisher: ETH Zurich. DOI: 10.3929/ETHZ-B-000343089. [Online]. Available: http://hdl.handle.net/20.500.11850/343089 (visited on 08/05/2022).

[35] K. E. Berg, K. M. Clark, X. Li, E. M. Carter, J. Volckens, and C. S. Henry, "High-throughput, semi-automated dithiothreitol (DTT) assays for oxidative potential of fine particulate matter," en, *Atmospheric Environment*, vol. 222, p. 117 132, Feb. 2020, ISSN: 13522310. DOI: 10.1016/j.atmosenv.2019.117132. [Online]. Available: https://linkinghub.elsevier.com/retrieve/pii/S135223101930771X (visited on 08/05/2022).

[36] T. Fang, V. Verma, H. Guo, L. E. King, E. S. Edgerton, and R. J. Weber, "A semi-automated system for quantifying the oxidative potential of ambient particles in aqueous extracts using the dithiothreitol (DTT) assay: Results from the Southeastern Center for Air Pollution and Epidemiology (SCAPE)," en, *Atmospheric Measurement Techniques*, vol. 8, no. 1, pp. 471–482, Jan. 2015, ISSN: 1867-8548. DOI: 10.5194/amt-8-471-2015. [Online]. Available: https://amt.copernicus.org/articles/8/471/2015/ (visited on 08/05/2022).

[37] A. Eiguren-Fernandez, N. Kreisberg, and S. Hering, "An online monitor of the oxidative capacity of aerosols (o-MOCA)," en, *Atmospheric Measurement Techniques*, vol. 10, no. 2, pp. 633–644, Feb. 2017, ISSN: 1867-8548. DOI: 10.5194/amt-10-633-2017. [Online]. Available: https://amt.copernicus.org/articles/10/633/2017/ (visited on 08/05/2022).

[38] J. V. Puthussery, C. Zhang, and V. Verma, "Development and field testing of an online instrument for measuring the real-time oxidative potential of ambient particulate matter based on dithiothreitol assay," en, *Atmospheric Measurement Techniques*, vol. 11, no. 10, pp. 5767–5780, Oct. 2018, ISSN: 1867-8548. DOI: 10.5194/amt-11-5767-2018. [Online]. Available: https://amt.copernicus.org/articles/11/5767/2018/ (visited on 08/05/2022).

[39] M. Takeuchi, S. M. R. Ullah, P. K. Dasgupta, D. R. Collins, and A. Williams, "Continuous Collection of Soluble Atmospheric Particles with a Wetted Hydrophilic Filter," en, *Analytical Chemistry*, vol. 77, no. 24, pp. 8031–8040, Dec. 2005, ISSN: 0003-2700, 1520-6882. DOI: 10.1021/ac051539o. [Online]. Available: https://pubs.acs.org/doi/10.1021/ac051539o (visited on 08/05/2022).

[40] F. O. f. t. E. FOEN, *Data query NABEL*, en. [Online]. Available: https://www.bafu.admin.ch/bafu/en/home/themen/thema-luft/luft--daten--indikatoren-und-karten/luftbelastung--daten/datenabfrage-nabel.html (visited on 06/28/2022).

[41] ——, *National Air Pollution Monitoring Network (NABEL)*, en. [Online]. Available: https://www.bafu.admin.ch/bafu/en/home/themen/thema-luft/luft--daten--indikatoren-und-karten/luftbelastung--daten/nationales-beobachtungsnetz-fuer-luftfremdstoffe--nabel-.html (visited on 06/28/2022).

[42] EMPA, *Empa - Air Pollution / Environmental Technology - Ambient Air Pollution / NABEL*. [Online]. Available: https://www.empa.ch/web/s503/nabel (visited on 06/28/2022).

[43] *RStudio — Open source & professional software for data science teams*, en. [Online]. Available: https://www.rstudio.com/ (visited on 06/29/2022).

[44] J. W. Tukey, *Exploratory data analysis*, ser. Addison-Wesley series in behavioral science. Reading, Mass: Addison-Wesley Pub. Co, 1977, ISBN: 978-0-201-07616-5.

[45] S. Reimann, *Air Pollution and Climate change: Measurements of atmospheric trace gases (EPFL course)*, Eglish, Feb. 2021.

[46] O. US EPA, *Basic Information about NO2*, en, Overviews and Factsheets, Jul. 2016. [Online]. Available: https://www.epa.gov/no2-pollution/basic-information-about-no2 (visited on 08/21/2022).